Journal of Computational Physics 556 (2026) 114813

Contents lists available at ScienceDirect

Journal of Computational Physics

journal homepage: www.elsevier.com/locate/jcp

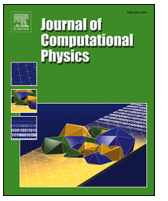

Computing the Bogoliubov-de Gennes excitations of two-component Bose-Einstein condensates

Manting Xie [a], Yong Zhang [b,c,*]

[a] School of Mathematics and KL-AAGDM, Tianjin University, 300350, Tianjin, China
[b] Center for Applied Mathematics and KL-AAGDM, Tianjin University, 300072, Tianjin, China
[c] State Key Laboratory of Synthetic Biology, Tianjin University, 300072, Tianjin, China

ARTICLE INFO

Keywords:
Two-component Bose-Einstein condensates
Bogoliubov-de Gennes excitations
Fourier spectral method
Bi-orthogonal structure-preserving
Large-scale eigenvalue problem

ABSTRACT

In this paper, we present an efficient and spectrally accurate numerical method to compute elementary/collective excitations in two-component Bose-Einstein condensates (BEC), around their mean-field ground state, by solving the associated Bogoliubov-de Gennes (BdG) equation. The BdG equation is essentially an eigenvalue problem for a non-Hermitian differential operator with an eigenfunction normalization constraint. Firstly, we investigate its analytical properties, including the exact eigenpairs, generalized nullspace structure and bi-orthogonality of eigenspaces. Subsequently, by combining the Fourier spectral method for spatial discretization and a stable modified Gram-Schmidt bi-orthogonal algorithm, we propose a structure-preserving iterative method for the resulting large-scale dense non-Hermitian discrete eigenvalue problem. Our method is matrix-free, and the matrix-vector multiplication (or the operator-function evaluation) is implemented with a near-optimal complexity $\mathcal{O}(N_t \log(N_t))$, where N_t is the total number of grid points, thanks to the utilization of the discrete Fast Fourier Transform (FFT). Therefore, it is memory-friendly, spectrally accurate, and highly efficient. Finally, we carry out a comprehensive numerical investigation to showcase its superiority in terms of accuracy and efficiency, alongside some applications to compute the excitation spectrum and Bogoliubov amplitudes in one, two, and three-dimensional problems.

1. Introduction

Early in 1996, right after the first realization of Bose-Einstein Condensations (BEC), researchers created a two-component BEC using the $|F = 2, m = 2\rangle$ and $|F = 1, m = -1\rangle$ states of ^{87}Rb via a double magneto-optic trap [1]. This experiment demonstrated the simultaneous cooling of two condensates and observed inter-component interactions. Building on this work, it was proposed that binary BEC systems could generate coherent matter waves, or atom lasers, similar to the coherent light emitted by lasers, driving significant interest in multi-component BEC systems. Subsequent physical experiments have discovered unique quantum phenomena, such as coherent atom transfer between hyperfine states and the emergence of density and spin oscillation modes along with a stable equilibrium [2–6].

* Corresponding author .
E-mail addresses: mtxie@tju.edu.cn (M. Xie), sunny5zhang@gmail.com, sunny5zhang@163.com, Zhang_Yong@tju.edu.cn (Y. Zhang).

https://doi.org/10.1016/j.jcp.2026.114813
Received 23 August 2025; Received in revised form 12 February 2026; Accepted 24 February 2026
Available online 26 February 2026

At temperature T much smaller than the critical temperature T_c [7–9], the two-component BEC is well described by the following coupled Gross-Pitaevskii equations (CGPEs)

$$i\partial_t\psi_1 = \Big[-\frac{1}{2}\nabla^2 + V(\boldsymbol{x}) + \frac{\delta}{2} + \Big(\beta_{11}|\psi_1|^2 + \beta_{12}|\psi_2|^2\Big)\Big]\psi_1 + \frac{\Omega}{2}\psi_2, \tag{1.1a}$$

$$i\partial_t\psi_2 = \Big[-\frac{1}{2}\nabla^2 + V(\boldsymbol{x}) - \frac{\delta}{2} + \Big(\beta_{21}|\psi_1|^2 + \beta_{22}|\psi_2|^2\Big)\Big]\psi_2 + \frac{\Omega}{2}\psi_1, \tag{1.1b}$$

where $t > 0$ denotes time and $\boldsymbol{x} = x$, $\boldsymbol{x} = (x, y)^\top$ and $\boldsymbol{x} = (x, y, z)^\top$ is the Cartesian coordinate vector, $\Psi(\boldsymbol{x}, t) = (\psi_1(\boldsymbol{x}, t), \psi_2(\boldsymbol{x}, t))^\top$ is the complex-valued macroscopic wave function corresponding to the spin-up and spin-down components, $V(\boldsymbol{x})$ is a real-valued external potential that is case-dependent, and one common choice is the harmonic trapping potential, which reads as

$$V(\boldsymbol{x}) = \frac{1}{2}\begin{cases} \gamma_x^2 x^2, & d = 1, \\ \gamma_x^2 x^2 + \gamma_y^2 y^2, & d = 2, \\ \gamma_x^2 x^2 + \gamma_y^2 y^2 + \gamma_z^2 z^2, & d = 3, \end{cases} \tag{1.2}$$

where γ_x, γ_y and γ_z are the trapping frequencies in x-, y- and z-directions, respectively, Ω is the effective Rabi frequency to realize the internal atomic Josephson junction (JJ) by a Raman transition, δ is the Raman transition constant, and β_{jl} (with $\beta_{jl} = \beta_{lj}$) are the effective interaction strength between the j-th and l-th components (positive for repulsive interaction and negative for attractive interaction).

The CGPEs (1.1a)-(1.1b) conserve two important quantities: the *mass*

$$\mathcal{N}(\Psi(\cdot, t)) := \|\Psi(\cdot, t)\|^2 = \sum_j \int_{\mathbb{R}^d} |\psi_j(\boldsymbol{x}, t)|^2 \mathrm{d}\boldsymbol{x} = 1, \quad t \geq 0, \tag{1.3}$$

and the *energy*

$$\mathcal{E}_\Omega(\Psi(\cdot, t)) = \int_{\mathbb{R}^d} \sum_j \frac{1}{2}|\nabla\psi_j|^2 + V(\boldsymbol{x})|\psi_j|^2 + \sum_{j,l}\frac{\beta_{jl}}{2}|\psi_j|^2|\psi_l|^2 + \frac{\delta}{2}\big(|\psi_1|^2 - |\psi_2|^2\big) + \Omega\,\mathfrak{Re}(\psi_1\overline{\psi_2})\,\mathrm{d}\boldsymbol{x}, \tag{1.4}$$

where $\bar{f}$ and $\mathfrak{Re}(f)$ denotes the conjugate and real part of the complex-valued function $f(\boldsymbol{x})$ respectively. In fact, we can construct stationary states $\Phi = (\phi_1, \phi_2)^\top$ of Eqs. (1.1a)-(1.1b) in the following way

$$\Psi(\boldsymbol{x}, t) = e^{-\mathrm{i}\mu t}\,\Phi(\boldsymbol{x}), \tag{1.5}$$

where Φ and μ (the chemical potential) are solutions to the following Euler-Lagrange equations (a type of nonlinear eigenvalue problem):

$$\mu\,\phi_1 = H_1\phi_1 := \Big[-\frac{1}{2}\nabla^2 + V(\boldsymbol{x}) + \frac{\delta}{2} + \big(\beta_{11}|\phi_1|^2 + \beta_{12}|\phi_2|^2\big)\Big]\phi_1 + \frac{\Omega}{2}\phi_2, \tag{1.6a}$$

$$\mu\,\phi_2 = H_2\phi_2 := \Big[-\frac{1}{2}\nabla^2 + V(\boldsymbol{x}) - \frac{\delta}{2} + \big(\beta_{21}|\phi_1|^2 + \beta_{22}|\phi_2|^2\big)\Big]\phi_2 + \frac{\Omega}{2}\phi_1, \tag{1.6b}$$

under the constraint $\mathcal{N}(\Phi) := \|\Phi\|^2 = 1$. The ground state, denoted by $\Phi_g = (\phi_1^g, \phi_2^g)^\top$, is a stationary state with the lowest energy and can also be defined as the minimizer of the following non-convex optimization problem

$$\Phi_g = \arg\min_{\Phi \in S_M} \mathcal{E}_\Omega(\Phi), \tag{1.7}$$

where the constraint functional space S_M reads

$$S_M := \Big\{\Phi = (\phi_1, \phi_2)^\top \;\Big|\; \mathcal{N}(\Phi) = 1,\ \mathcal{E}_\Omega(\Phi) < \infty\Big\}.$$

For the case without internal Josephson junction ($\Omega = 0$), the mass of each component is conserved, that is,

$$\int_{\mathbb{R}^d} |\psi_1(\boldsymbol{x}, 0)|^2 \mathrm{d}\boldsymbol{x} = \alpha \quad \text{and} \quad \int_{\mathbb{R}^d} |\psi_2(\boldsymbol{x}, 0)|^2 \mathrm{d}\boldsymbol{x} = 1 - \alpha, \quad \alpha \in [0, 1]. \tag{1.8}$$

The stationary state satisfies the following Euler-Lagrange equations

$$\mu_1\,\phi_1 = \Big[-\frac{1}{2}\nabla^2 + V(\boldsymbol{x}) + \frac{\delta}{2} + \big(\beta_{11}|\phi_1|^2 + \beta_{12}|\phi_2|^2\big)\Big]\phi_1, \tag{1.9a}$$

$$\mu_2\,\phi_2 = \Big[-\frac{1}{2}\nabla^2 + V(\boldsymbol{x}) - \frac{\delta}{2} + \big(\beta_{21}|\phi_1|^2 + \beta_{22}|\phi_2|^2\big)\Big]\phi_2, \tag{1.9b}$$

under constraints $\|\phi_1\|^2 = \alpha$, $\|\phi_2\|^2 = 1-\alpha$ with μ_1 and μ_2 being the chemical potentials associated with each component. The ground state and its corresponding chemical potential, denoted by $\Phi_g^\alpha(\boldsymbol{x}) = (\phi_1^\alpha, \phi_2^\alpha)^\top$ and μ_1^α & μ_2^α, could also be defined as the minimizer of the following problem

$$\Phi_g^\alpha = \arg\min_{\Phi \in S_M^\alpha} \mathcal{E}_0(\Phi), \tag{1.10}$$

where S_M^α is a nonconvex set defined as

$$S_M^\alpha := \Big\{\Phi = (\phi_1, \phi_2)^\top \;\Big|\; \|\phi_1\|^2 = \alpha,\ \|\phi_2\|^2 = 1 - \alpha,\ \mathcal{E}_0(\Phi) < \infty\Big\}. \tag{1.11}$$

The CGPEs (1.1a)-(1.1b) hold for the two-component BEC at the mean-field level [7,8]. Nonetheless, due to the many-body effects stemming from interatomic interactions, excitations are observed even in the ground state. These excitations can be treated as quasi-particles and are named as elementary or collective excitations [10]. To properly account for such excitations, one must extend beyond mean-field theory. The Bogoliubov theory provides a perturbative analysis around the ground state, ultimately leading to an eigenvalue problem – the renowned Bogoliubov-de Gennes (BdG) equation [11–14].

Since the first observations of excitation modes [15], there has been a significant growing interest in mathematical and numerical studies devoted to the Bogoliubov-de Gennes (BdG) equations over the past few decades [16–18]. Along the numerical front, various research utilized the standard ARPACK library [19] to solve the BdG equations for different types of BEC. For an incomplete list of references, see [12,20–22]. For problems in lower dimensions ($d = 1, 2$), the resulting eigenvalue problems are typically solved using direct eigenvalue solvers, such as MATLAB's "eigs" function, or iterative subspace solvers like those provided by ARPACK, or locally optimal block-preconditioned conjugate gradient methods [23,24].

To date, there are quite few mathematical studies, and most numerical investigations have concentrated on lower-dimensional scenarios ($d = 1$ or 2), for example, the low-lying elementary (or collective) excitations in quasi-two-dimensional rotating systems [12,25]. Chen et al. [26] employed the Arnoldi method to directly solve the BdG equations for spin-orbit coupled BEC, and Sadaka et al. [27] developed a numerical eigenvalue solver with FreeFEM and ARPACK. More recently, a series of spectrally accurate eigenvalue solvers were proposed for dipolar/spin-1 BEC based on ARPACK or Bi-Orthogonal Structure-Preserving solver (BOSP) [28] in high space dimension [22,25,29].

So far as we know, when solving BdG equations numerically, two major challenges arise: (i) the development of an accurate stationary state solver; (ii) the design of an accurate and efficient eigensolver for the BdG equation. For the stationary/ground state computation, several numerical methods have been proposed, including the gradient flow method [8,30,31], regularized Newton method [32] and Preconditioned Conjugate Gradient (PCG) method [33] etc. Here, in this article, we choose PCG [33] for its excellent performance in accuracy, efficiency and robustness. While the BdG equation generally admits eigenvalue zero, and, for current popular eigensolvers, the most challenging tasks consist of the convergence at eigenvalue zero and the overall computational efficiency that usually bottlenecks numerical simulation, especially in high spatial dimensions.

It is well known that the eigenvalue distribution and structure of the generalized nullspace are of essential importance to the design of eigensolvers to achieve better performance. For the BdG equation, all the eigenvalues come in negative/positive pairs along the real line, and the eigenspaces associated with eigenvalues of different magnitudes are bi-orthogonal to each other [28]. While for eigenvalue zero, the algebraic multiplicity is usually greater than its geometric counterpart, therefore, the generalized nullspace has a very complicated structure. Yet, not all such intrinsic properties and structures have been adequately taken into account in current solvers. Simple adaptation of existing solvers, for example, ARPACK [19] and LOBP4DCG [23,24], might suffer from slow convergence or even divergence, especially when there is an eigenvalue of zero, and the performance is much more likely to degrade significantly in large-scale computation. To make it worse, the eigenfunctions are typically discretized with the Fourier spectral method, leading to a fully populated dense eigensystem, and explicit matrix storage incurs prohibitive memory costs, especially for high-dimensional problems. Therefore, it is imperative to develop an iterative algorithm where the user can provide a matrix-vector product implementation, waiving any explicit matrix storage, thus enabling computation of large-scale problems in high space dimensions.

Recently, the BOSP algorithm, proposed by Li et al [28], successfully incorporated the eigenspaces' bi-orthogonality using a modified Gram-Schmidt bi-orthogonalization algorithm, achieving great efficiency and parallel scalability. Moreover, it provided an interactive interface through which the users are allowed to implement their matrix-vector product. It shall perform better if the generalized nullspaces could be given *a priori* whenever possible. In this article, to adapt BOSP for our problem, we shall first investigate the structure of generalized nullspace on analytical level, then design an efficient matrix-vector product, which should be an accurate approximation of operator-function evaluation, aiming to achieve spectral-accuracy computation of all non-zero eigenvalues and their corresponding eigenfunctions.

Overall, the main objectives of this paper are as follows:

(1) derive the Bogoliubov-de Gennes (BdG) equation for two-component BEC around the ground state and investigate its mathematical structures, including analytical eigenvalues/eigenfunctions, the generalized nullspace, and the bi-orthogonality of eigenspaces;
(2) develop a bi-orthogonal structure-preserving Fourier spectral method and propose an effective implementation for evaluating the matrix-vector product based on Fourier spectral method and FFT;
(3) verify the spectral accuracy, efficiency, and scalability of the method, and numerically study the excitation spectrum and Bogoliubov amplitudes around the ground state for different parameters in one/two/three-dimensional (1D, 2D and 3D) settings.

The rest of the paper is organized as follows: In Section 2, we introduce the BdG equations and derive some analytical properties. In Section 3, we present details of the Fourier spectral method for space discretization and propose an efficient numerical method. Extensive numerical examples are shown in Section 4 to confirm the performance of our method, together with some applications to study the solutions to the BdG equations with different parameters in 1D–3D. Finally, conclusions are drawn in Section 5.

2. The BdG equation and its properties

2.1. The Bogoliubov-de Gennes equations

To characterize the elementary/collective excitations of a two-component BEC, the Bogoliubov theory [11,12] begins with the stationary state Φ of the CGPEs (1.1a)-(1.1b) with an internal atomic Josephson junction ($\Omega \neq 0$), which is also an solution to the nonlinear eigenvalue problems (1.6a)-(1.6b) with corresponding chemical potential μ, and assumes the evolution is around state Φ. The corresponding wave function Ψ takes the following form [22,34]

$$\Psi(\boldsymbol{x},t) = \exp(-\mathrm{i}\mu t)\left[\Phi(\boldsymbol{x}) + \varepsilon \sum_{\ell=1}^{\infty}\left(\boldsymbol{u}^{\ell}(\boldsymbol{x})e^{-\mathrm{i}\omega_{\ell}t} + \bar{\boldsymbol{v}}^{\ell}(\boldsymbol{x})e^{\mathrm{i}\omega_{\ell}t}\right)\right], \ \boldsymbol{x}\in\mathbb{R}^d, \ t>0. \tag{2.1}$$

Here, $0<\varepsilon\ll 1$ is a small quantity used to control the population of quasiparticle excitation, $\boldsymbol{\omega}_{\ell}\in\mathbb{R}$ is the frequency of the excitations to be determined, and $\boldsymbol{u}^{\ell},\boldsymbol{v}^{\ell}\in H^1(\mathbb{R}^d;\mathbb{C}^2)$ are the Bogoliubov excitation modes satisfying normalization condition

$$\int_{\mathbb{R}^d}\left(|\boldsymbol{u}^{\ell}(\boldsymbol{x})|^2 - |\boldsymbol{v}^{\ell}(\boldsymbol{x})|^2\right)\mathrm{d}\boldsymbol{x} = \int_{\mathbb{R}^d}\sum_{j}\left(|u_j^{\ell}(\boldsymbol{x})|^2 - |v_j^{\ell}(\boldsymbol{x})|^2\right)\mathrm{d}\boldsymbol{x} = 1, \quad \ell\in\mathbb{Z}^+. \tag{2.2}$$

where $\boldsymbol{u}^{\ell} = (u_1^{\ell},u_2^{\ell})^{\top}, \boldsymbol{v}^{\ell} = (v_1^{\ell},v_2^{\ell})^{\top}$. Plugging (2.1) into Eqs. (1.1a)-(1.1b), by collecting linear terms in ε and separating frequency $e^{-\mathrm{i}\omega_{\ell}t}$ and $e^{\mathrm{i}\omega_{\ell}t}$, we obtain the BdG equations as follows

$$\mathcal{L}\begin{bmatrix}\boldsymbol{u}\\ \boldsymbol{v}\end{bmatrix} := \begin{bmatrix}\mathcal{A} & \mathcal{B}\\ C & \mathcal{D}\end{bmatrix}\begin{bmatrix}\boldsymbol{u}\\ \boldsymbol{v}\end{bmatrix} = \omega\begin{bmatrix}\boldsymbol{u}\\ \boldsymbol{v}\end{bmatrix}, \tag{2.3}$$

with constraint

$$\int_{\mathbb{R}^d}\left(|\boldsymbol{u}(\boldsymbol{x})|^2 - |\boldsymbol{v}(\boldsymbol{x})|^2\right)\mathrm{d}\boldsymbol{x} = 1, \tag{2.4}$$

where all the subscripts ℓ are omitted hereafter for simplicity, ω is the excitation energy and the operators are given explicitly

$$\mathcal{A} := \begin{bmatrix}L_1 & \beta_{12}\phi_1\overline{\phi_2} + \frac{\Omega}{2}\\ \beta_{21}\overline{\phi_1}\phi_2 + \frac{\Omega}{2} & L_2\end{bmatrix}, \ \mathcal{B} := \begin{bmatrix}\beta_{11}(\phi_1)^2 & \beta_{12}\phi_1\phi_2\\ \beta_{21}\phi_1\phi_2 & \beta_{22}(\phi_2)^2\end{bmatrix}, \tag{2.5}$$

$$C := -\begin{bmatrix}\beta_{11}(\overline{\phi_1})^2 & \beta_{12}\overline{\phi_1\phi_2}\\ \beta_{21}\overline{\phi_1\phi_2} & \beta_{22}(\overline{\phi_2})^2\end{bmatrix}, \ \mathcal{D} := -\begin{bmatrix}L_1 & \beta_{12}\overline{\phi_1}\phi_2 + \frac{\Omega}{2}\\ \beta_{21}\phi_1\overline{\phi_2} + \frac{\Omega}{2} & L_2\end{bmatrix}, \tag{2.6}$$

with

$$L_1 = -\frac{1}{2}\nabla^2 + V(\boldsymbol{x}) + \frac{\delta}{2} + 2\beta_{11}|\phi_1|^2 + \beta_{12}|\phi_2|^2 - \mu_g,$$
$$L_2 = -\frac{1}{2}\nabla^2 + V(\boldsymbol{x}) - \frac{\delta}{2} + \beta_{21}|\phi_1|^2 + 2\beta_{22}|\phi_2|^2 - \mu_g.$$

It is easy to check that $\mathcal{A}$ and D are both Hermitian operators, i.e., $\mathcal{A}^* = \mathcal{A}$, $\mathcal{D}^* = \mathcal{D}$, and $\mathcal{B}^* = -C$, where symbol $*$ denotes the adjoint operator associated with **inner product** $\langle \boldsymbol{f},\boldsymbol{g}\rangle := \sum_{j=1,2}\int_{\mathbb{R}^d} f_j(\boldsymbol{x})\overline{g_j(\boldsymbol{x})}\,\mathrm{d}\boldsymbol{x}$. Furthermore, we have $\overline{\mathcal{A}\boldsymbol{g}} = -\mathcal{D}\bar{\boldsymbol{g}}$, $\overline{\mathcal{B}\boldsymbol{g}} = -C\bar{\boldsymbol{g}}$, $\forall\,\boldsymbol{g}\in H^1(\mathbb{R}^d;\mathbb{C}^2)$, and it immediately implies the operators' finite-dimensional subspace representations, denoted by matrices A, B, C and D, are either Hermitian or symmetric, that is,

$$A^{\mathsf{H}} = A, \quad D = -\overline{A}, \quad B^{\top} = B \quad \text{and} \quad C = -\overline{B}. \tag{2.7}$$

The matrices representation of (2.3) reads as follows

$$\begin{bmatrix}A & B\\ -\overline{B} & -\overline{A}\end{bmatrix}\begin{bmatrix}\mathbf{u}\\ \mathbf{v}\end{bmatrix} = \omega\begin{bmatrix}\mathbf{u}\\ \mathbf{v}\end{bmatrix}, \tag{2.8}$$

and it coincides with the Bethe-Salpeter Hamiltonian (BSH) matrix arising from optical absorption spectrum analysis [35].

Similarly, if there is no internal atomic Josephson junction (i.e. $\Omega = 0$) in Eqs. (1.1a)-(1.1b), for any given $\alpha\in[0,1]$, the corresponding wave function Ψ takes the following form [22,34]

$$\Psi(\boldsymbol{x},t) = \mathrm{diag}\left(\exp(-\mathrm{i}\mu_1^{\alpha}t), \exp(-\mathrm{i}\mu_2^{\alpha}t)\right)\left[\Phi_g^{\alpha}(\boldsymbol{x}) + \varepsilon\sum_{\ell=1}^{\infty}\left(\boldsymbol{u}^{\ell}(\boldsymbol{x})e^{-\mathrm{i}\omega_{\ell}t} + \bar{\boldsymbol{v}}^{\ell}(\boldsymbol{x})e^{\mathrm{i}\omega_{\ell}t}\right)\right], \ \boldsymbol{x}\in\mathbb{R}^d, \ t>0, \tag{2.9}$$

and obtain the following similar BdGEs:

$$\mathcal{L}_{\alpha}\begin{bmatrix}\boldsymbol{u}\\ \boldsymbol{v}\end{bmatrix} := \begin{bmatrix}\mathcal{A}_{\alpha} & \mathcal{B}_{\alpha}\\ C_{\alpha} & \mathcal{D}_{\alpha}\end{bmatrix}\begin{bmatrix}\boldsymbol{u}\\ \boldsymbol{v}\end{bmatrix} = \omega\begin{bmatrix}\boldsymbol{u}\\ \boldsymbol{v}\end{bmatrix}, \tag{2.10}$$

with constraint (2.4), where ω is the excitation energy corresponding to the excitation mode $(\boldsymbol{u}^\top, \boldsymbol{v}^\top)^\top$ and and $\mathcal{A}_\alpha$, $\mathcal{B}_\alpha$, $\mathcal{C}_\alpha$ and $\mathcal{D}_\alpha$ are defined as

$$\mathcal{A}_\alpha = \begin{bmatrix} L_1^\alpha & \beta_{12}\phi_1^\alpha\overline{\phi_2^\alpha} \\ \beta_{21}\overline{\phi_1^\alpha}\phi_2^\alpha & L_2^\alpha \end{bmatrix}, \quad \mathcal{B}_\alpha = \begin{bmatrix} \beta_{11}(\phi_1^\alpha)^2 & \beta_{12}\phi_1^\alpha\phi_2^\alpha \\ \beta_{21}\phi_1^\alpha\phi_2^\alpha & \beta_{22}(\phi_2^\alpha)^2 \end{bmatrix},$$
$$\mathcal{C}_\alpha = -\begin{bmatrix} \beta_{11}(\overline{\phi_1^\alpha})^2 & \beta_{12}\overline{\phi_1^\alpha}\overline{\phi_2^\alpha} \\ \beta_{21}\overline{\phi_1^\alpha}\overline{\phi_2^\alpha} & \beta_{22}(\overline{\phi_2^\alpha})^2 \end{bmatrix}, \quad \mathcal{D}_\alpha = -\begin{bmatrix} L_1^\alpha & \beta_{12}\overline{\phi_1^\alpha}\phi_2^\alpha \\ \beta_{21}\phi_1^\alpha\overline{\phi_2^\alpha} & L_2^\alpha \end{bmatrix},$$

with

$$L_1^\alpha = -\frac{1}{2}\nabla^2 + V(\boldsymbol{x}) + \frac{\delta}{2} + 2\beta_{11}|\phi_1^\alpha|^2 + \beta_{12}|\phi_2^\alpha|^2 - \mu_1^\alpha,$$
$$L_2^\alpha = -\frac{1}{2}\nabla^2 + V(\boldsymbol{x}) - \frac{\delta}{2} + \beta_{21}|\phi_1^\alpha|^2 + 2\beta_{22}|\phi_2^\alpha|^2 - \mu_2^\alpha.$$

2.2. Analytical properties

In this subsection, we derive some analytical properties of the BdG equations as well as the structure of eigenfunctions for the two-component BEC with internal atomic Josephson junction ($\Omega \neq 0$), which might serve as benchmarks for numerical solutions or help to design an efficient numerical method for eigenvalue problems.

Here, it should be noted that although the establishment of the model requires ω to be a real number, for the following model eigenvalue problem

$$\begin{bmatrix} \mathcal{A} & \mathcal{B} \\ \mathcal{C} & \mathcal{D} \end{bmatrix}\begin{bmatrix} \boldsymbol{u} \\ \boldsymbol{v} \end{bmatrix} = \lambda\begin{bmatrix} \boldsymbol{u} \\ \boldsymbol{v} \end{bmatrix}, \tag{2.11}$$

its eigenvalue λ may be complex. Thus, we have the following theorem:

Theorem 1 (Symmetric distribution). *If $\{\lambda; \boldsymbol{u}, \boldsymbol{v}\}(\lambda \in \mathbb{C})$ is a solution pair to the eigenvalue problem (2.11), then $\{-\bar{\lambda}; \bar{\boldsymbol{v}}, \bar{\boldsymbol{u}}\}$ is also a solution pair. Furthermore, if $(\boldsymbol{u}, \boldsymbol{v})$ satisfies the normalization constraint (2.4), the corresponding eigenvalue of (2.3) is real, that is, $\omega \in \mathbb{R}$.*

Proof. The first conclusion can be proved by taking the conjugate of Eq. (2.11). Multiplying the first/second equation of (2.3) by $\boldsymbol{u}/\boldsymbol{v}$ respectively and integrating each equation concerning $\boldsymbol{x}$, we subtract the second integration from the first one to obtain the following

$$\langle \mathcal{A}\boldsymbol{u}, \boldsymbol{u}\rangle + \langle \mathcal{B}\boldsymbol{v}, \boldsymbol{u}\rangle - \langle \mathcal{C}\boldsymbol{u}, \boldsymbol{v}\rangle - \langle \mathcal{D}\boldsymbol{v}, \boldsymbol{v}\rangle = \omega \int_{\mathbb{R}^d} (|\boldsymbol{u}(\boldsymbol{x})|^2 - |\boldsymbol{v}(\boldsymbol{x})|^2)\,\mathrm{d}\boldsymbol{x}. \tag{2.12}$$

From Eq. (2.4), we can see that ω is real. □

Theorem 2 (Analytical eigenpairs). *Let $\Phi = (\phi_1, \phi_2)^\top$ be a stationary state for Eqs. (1.1a)-(1.1b) with harmonic trapping potential (1.2), we have analytical solutions to the BdG Eq. (2.3) as follows*

$$\{\omega_\sigma; \boldsymbol{u}_\sigma, \boldsymbol{v}_\sigma\} := \left\{\gamma_\sigma; \frac{1}{\sqrt{2}}\left(\gamma_\sigma^{-\frac{1}{2}}\partial_\sigma\Phi - \gamma_\sigma^{\frac{1}{2}}\sigma\Phi\right), \frac{1}{\sqrt{2}}\left(\gamma_\sigma^{-\frac{1}{2}}\partial_\sigma\overline{\Phi} + \gamma_\sigma^{\frac{1}{2}}\sigma\overline{\Phi}\right)\right\}, \tag{2.13}$$

with $\sigma = x$ in one dimension, $\sigma = x, y$ in two dimensions and $\sigma = x, y, z$ in three dimensions.

Proof.

For simplicity, we only prove the $\sigma = x$ case, and extensions to other spatial variables are similar. Differentiate Eqs. (1.6a)-(1.6b) with respect to x, we derive

$$L_1(\partial_x\phi_1) + \gamma_x^2 x\phi_1 + \beta_{11}(\phi_1)^2(\partial_x\overline{\phi_1}) + \beta_{12}\left[\phi_1\overline{\phi_2}(\partial_x\phi_2) + \phi_1\phi_2(\partial_x\overline{\phi_2})\right] + \frac{\Omega}{2}\partial_x\phi_2 = 0, \tag{2.14}$$
$$L_2(\partial_x\phi_2) + \gamma_x^2 x\phi_2 + \beta_{21}\left[\overline{\phi_1}\phi_2(\partial_x\phi_2) + \phi_1\phi_2(\partial_x\overline{\phi_1})\right] + \beta_{22}(\phi_2)^2(\partial_x\overline{\phi_2}) + \frac{\Omega}{2}\partial_x\phi_1 = 0. \tag{2.15}$$

Multiply both sides of Eqs. (1.6a)-(1.6b) by $\gamma_x x$, we have

$$L_1(\gamma_x x\phi_1) - \beta_{11}|\phi_1|^2(\gamma_x x\phi_1) + \gamma_x(\partial_x\phi_1) + \frac{\Omega}{2}\gamma_x x\phi_2 = 0, \tag{2.16}$$
$$L_2(\gamma_x x\phi_2) - \beta_{22}|\phi_2|^2(\gamma_x x\phi_2) + \gamma_x(\partial_x\phi_2) + \frac{\Omega}{2}\gamma_x x\phi_1 = 0. \tag{2.17}$$

By subtracting Eq. (2.16) from Eq. (2.14) and Eq. (2.17) from Eq. (2.15), we get

$$\mathcal{A}(\partial_x\Phi - \gamma_x x\Phi) + \mathcal{B}(\partial_x\overline{\Phi} + \gamma_x x\overline{\Phi}) = \gamma_x(\partial_x\Phi - \gamma_x x\Phi). \tag{2.18}$$

Summing Eqs. (2.14) & (2.16) and Eqs. (2.15) & (2.17), and taking complex conjugates, we obtain

$$\mathcal{C}(\partial_x\Phi - \gamma_x x\Phi) + \mathcal{D}(\partial_x\overline{\Phi} + \gamma_x x\overline{\Phi}) = \gamma_x(\partial_x\overline{\Phi} + \gamma_x x\overline{\Phi}). \tag{2.19}$$

Therefore, we can verify that $\{\partial_x\Phi - \gamma_x x\Phi, \partial_x\overline{\Phi} + \gamma_x x\overline{\Phi}\}$ solves (2.21) with $\omega = \gamma_x$.

Simple calculations lead to the following identity

$$\int_{\mathbb{R}^d} \left(|\partial_x \Phi - \gamma_x x\Phi|^2 - |\partial_x \overline{\Phi} + \gamma_x x\overline{\Phi}|^2 \right) \mathrm{d}\boldsymbol{x} = -2 \int_{\mathbb{R}^d} \left(\gamma_x x\Phi \partial_x \overline{\Phi} + \gamma_x x\overline{\Phi} \partial_x \Phi \right) \mathrm{d}\boldsymbol{x} = 2\gamma_x,$$

then we derive the analytical solutions as

$$\omega_x = \gamma_x, \quad \boldsymbol{u}_x = \frac{1}{\sqrt{2}} \left(\gamma_x^{-\frac{1}{2}} \partial_x \Phi - \gamma_x^{\frac{1}{2}} x\Phi \right), \quad \boldsymbol{v}_x = \frac{1}{\sqrt{2}} \left(\gamma_x^{-\frac{1}{2}} \partial_x \overline{\Phi} + \gamma_x^{\frac{1}{2}} x\overline{\Phi} \right).$$

□

As shown in [8], under appropriate assumptions, the ground state $\Phi_g = (\phi_1^g, \phi_2^g)^\top$ are **real-valued** functions. Therefore, we shall focus on the real ground state hereafter, and all operators involved are real. To be more specific,

$$\mathcal{D} = -\mathcal{A}, \quad \mathcal{C} = -\mathcal{B},$$

then the BdG Eq. (2.3) becomes a linear response problem of the following form

$$\begin{bmatrix} \mathcal{A} & \mathcal{B} \\ -\mathcal{B} & -\mathcal{A} \end{bmatrix} \begin{bmatrix} \boldsymbol{u} \\ \boldsymbol{v} \end{bmatrix} = \omega \begin{bmatrix} \boldsymbol{u} \\ \boldsymbol{v} \end{bmatrix}. \tag{2.20}$$

By applying a change of variables $\boldsymbol{u} = \boldsymbol{f} + \boldsymbol{g}$, $\boldsymbol{v} = \boldsymbol{f} - \boldsymbol{g}$, the above equation can be reformulated

$$\mathcal{H} \begin{bmatrix} \boldsymbol{f} \\ \boldsymbol{g} \end{bmatrix} := \begin{bmatrix} \mathcal{O} & \mathcal{H}_- \\ \mathcal{H}_+ & \mathcal{O} \end{bmatrix} \begin{bmatrix} \boldsymbol{f} \\ \boldsymbol{g} \end{bmatrix} = \omega \begin{bmatrix} \boldsymbol{f} \\ \boldsymbol{g} \end{bmatrix}, \tag{2.21}$$

where $\mathcal{H}_+ := \mathcal{A} + \mathcal{B}$ and $\mathcal{H}_- := \mathcal{A} - \mathcal{B}$ are both Hermitian operators, and the constraint (2.4) is reformulated as $\langle \boldsymbol{f}, \boldsymbol{g} \rangle = 1/4$. Eq. (2.21) immediately leads to two decoupled linear eigenvalue problems, that is,

$$\mathcal{H}_- \mathcal{H}_+ \boldsymbol{f} = \omega^2 \boldsymbol{f}, \qquad \mathcal{H}_+ \mathcal{H}_- \boldsymbol{g} = \omega^2 \boldsymbol{g}. \tag{2.22}$$

Theorem 3 (Bi-orthogonality). *Assume $\{\omega_i; \boldsymbol{f}_i, \boldsymbol{g}_i\}_{i=1}^2$ are eigenpairs of Eq. (2.21) with eigenvalues of different magnitudes, i.e., $|\omega_1| \neq |\omega_2|$, the following bi-orthogonal properties hold true*

$$\langle \boldsymbol{f}_1, \boldsymbol{g}_2 \rangle = \langle \boldsymbol{f}_2, \boldsymbol{g}_1 \rangle = 0.$$

Proof. Using Eq. (2.22), we have

$$\omega_i^2 \langle \boldsymbol{f}_i, \boldsymbol{g}_j \rangle = \langle \mathcal{H}_- \mathcal{H}_+ \boldsymbol{f}_i, \boldsymbol{g}_j \rangle = \langle \boldsymbol{f}_i, \mathcal{H}_+ \mathcal{H}_- \boldsymbol{g}_j \rangle = \omega_j^2 \langle \boldsymbol{f}_i, \boldsymbol{g}_j \rangle,$$

which means

$$(\omega_i^2 - \omega_j^2) \langle \boldsymbol{f}_i, \boldsymbol{g}_j \rangle = 0.$$

Since $|\omega_i| \neq |\omega_j|$, we obtain $\langle \boldsymbol{f}_i, \boldsymbol{g}_j \rangle = 0$, for $i \neq j$. □

Remark 1. In this subsection, we only focus on the case with an internal atomic Josephson junction ($\Omega \neq 0$). Actually, Theorems 1–3 also hold for the case without an internal atomic Josephson junction ($\Omega = 0$), and they are omitted here for brevity.

2.3. Generalized nullspace

As is known, the algebraic/geometric multiplicity of eigenvalue zero and the structure of its associated generalized nullspace are of great importance to the solver's performance in terms of convergence, accuracy and efficiency. The generalized nullspace of $\mathcal{H}$ is defined as nullspace of $\mathcal{H}^q$ for some positive integer p such that

$$\mathrm{null}(\mathcal{H}^p) = \mathrm{null}(\mathcal{H}^{p+1}).$$

For the operator $\mathcal{H}$, the integer p is finite and $\mathrm{null}(\mathcal{H}^p) = \mathrm{null}(\mathcal{H}^q)$ holds true for any greater integer q, i.e, $q \geq p$. In this subsection, we shall elaborate on the structure of the generalized nullspace, which is, of course, closely connected with the nullspace of $\mathcal{H}_-$ and $\mathcal{H}_+$.

2.3.1. With an internal atomic Josephson junction ($\Omega \neq 0$)

First and foremost, we shall present the conditions for the existence and uniqueness of the ground state solution of (1.7).

Lemma 1 (Existence and uniqueness of the ground state [7]). *Suppose $V(x) \geq 0$ satisfying $\lim_{|x|\to\infty} V(x) = \infty$ and at least one of the following conditions holds,*

(i) $d = 1$;
(ii) $d = 2$ *and* $\beta_{11} \geq C_b, \beta_{22} \geq -C_b$, *and* $\beta_{12} = \beta_{21} \geq -C_b - \sqrt{C_b + \beta_{11}}\sqrt{C_b + \beta_{22}}$;
(iii) $d = 3$ *and* $\begin{bmatrix} \beta_{11} & \beta_{12} \\ \beta_{21} & \beta_{22} \end{bmatrix}$ *is either positive semi-definite or nonnegative,*

there exists a ground state $\Phi_g = (\phi_1^g, \phi_2^g)^\top$ *of* (1.7). *Furthermore, if the matrix* $\begin{bmatrix} \beta_{11} & \beta_{12} \\ \beta_{21} & \beta_{22} \end{bmatrix}$ *is positive semi-definite and at least one of the parameters* δ, Ω, $\beta_{11} - \beta_{22}$ *and* $\beta_{11} - \beta_{12}$ *are nonzero, then the ground state* $(|\phi_1^g|, -\mathrm{sign}(\Omega)|\phi_2^g|)^\top$ *is unique.*

Theorem 4 (Nullspace of $\mathcal{H}_-$ for system with JJ ($\Omega \neq 0$))**.** *Under conditions of Lemma 1, we have the following property for nullspace of* $\mathcal{H}_-$

$$\mathrm{span}\{\Phi_g\} \subset \mathrm{null}(\mathcal{H}_-).$$

Proof. Just verify $\mathcal{H}_-\Phi_g = 0$ directly and omit the detailed proof here. □

Remark 2. From our extensive numerical results, not fully shown here, we conjecture that the following property holds for $\Omega \neq 0$:

$\mathcal{H}_+$ is positive definite and $\mathrm{null}(\mathcal{H}_-) = \mathrm{span}\{\Phi_g\}$.

Finally, we present the structure of the generalized nullspace of the operator $\mathcal{H}$.

Theorem 5 (Generalized nullspace of $\mathcal{H}$ for system with JJ ($\Omega \neq 0$))**.** *If the above property is true, we can obtain the generalized nullspace of* $\mathcal{H}$ *as follows*

$$\mathrm{null}(\mathcal{H}^3) = \mathrm{null}(\mathcal{H}^2) = \mathrm{null}(\mathcal{H}) \oplus \mathrm{span}\left\{ \begin{bmatrix} \hat{\Phi}_1 \\ \mathbf{0} \end{bmatrix} \right\}, \tag{2.23}$$

where $\hat{\Phi}_1 = \mathcal{H}_+^{-1}\Phi_g$, *and* $\mathrm{null}(\mathcal{H}) = \mathrm{span}\left\{ \begin{bmatrix} \mathbf{0} \\ \Phi_g \end{bmatrix} \right\}$.

Proof. It is easy to verify that

$$\mathrm{null}(\mathcal{H}) = \{(\boldsymbol{f}, \boldsymbol{g})^\top | \mathcal{H}_-\boldsymbol{g} = \mathbf{0}, \mathcal{H}_+\boldsymbol{f} = 0\} = \{(\mathbf{0}, \boldsymbol{g})^\top | \boldsymbol{g} \in \mathrm{null}(\mathcal{H}_-)\} = \mathrm{span}\left\{ \begin{bmatrix} \mathbf{0} \\ \Phi_g \end{bmatrix} \right\}.$$

For $\mathrm{null}(\mathcal{H}^2)$ and $\mathrm{null}(\mathcal{H}^3)$, we can obtain

$$\begin{aligned} \mathrm{null}(\mathcal{H}^2) &= \{(\boldsymbol{f}, \boldsymbol{g})^\top | \mathcal{H}_+\mathcal{H}_-\boldsymbol{g} = \mathbf{0}, \mathcal{H}_-\mathcal{H}_+\boldsymbol{f} = 0\} \\ &= \{(\boldsymbol{f}, \boldsymbol{g})^\top | \mathcal{H}_-\boldsymbol{g} = \mathbf{0}, \mathcal{H}_+\boldsymbol{f} \in \mathrm{null}(\mathcal{H}_-)\} \\ &= \{(\boldsymbol{f}, \boldsymbol{g})^\top | \boldsymbol{g} \in \mathrm{null}(\mathcal{H}_-), \boldsymbol{f} \in \mathcal{H}_+^{-1}\mathrm{null}(\mathcal{H}_-)\} \\ &= \mathrm{null}(\mathcal{H}) \oplus \mathrm{span}\left\{ \begin{bmatrix} \hat{\Phi}_1 \\ \mathbf{0} \end{bmatrix} \right\}, \end{aligned}$$

and

$$\begin{aligned} \mathrm{null}(\mathcal{H}^3) &= \{(\boldsymbol{f}, \boldsymbol{g})^\top | \mathcal{H}_-\mathcal{H}_+\mathcal{H}_-\boldsymbol{g} = \mathbf{0}, \mathcal{H}_+\mathcal{H}_-\mathcal{H}_+\boldsymbol{f} = 0\} \\ &= \{(\boldsymbol{f}, \boldsymbol{g})^\top | \mathcal{H}_-\boldsymbol{g} \in \mathcal{H}_+^{-1}\mathrm{null}(\mathcal{H}_-), \boldsymbol{f} \in \mathcal{H}_+^{-1}\mathrm{null}(\mathcal{H}_-)\}. \end{aligned}$$

Obviously, $\mathrm{null}(\mathcal{H}^2) \subset \mathrm{null}(\mathcal{H}^3)$. Next, we prove that $\mathrm{null}(\mathcal{H}^3) \subset \mathrm{null}(\mathcal{H}^2)$. For any $(\boldsymbol{f}, \boldsymbol{g})^\top \in \mathrm{null}(\mathcal{H}^3)$, i.e., $\mathcal{H}_-\boldsymbol{g} \in \mathcal{H}_+^{-1}\mathrm{null}(\mathcal{H}_-)$, we have $\mathcal{H}_-\boldsymbol{g} = c\,\hat{\Phi}_1$ and

$$0 = \langle \mathbf{0}, \boldsymbol{g} \rangle = \langle \mathcal{H}_-\Phi_g, \boldsymbol{g} \rangle = \langle \Phi_g, \mathcal{H}_-\boldsymbol{g} \rangle = \langle \mathcal{H}_+\hat{\Phi}_1, c\,\hat{\Phi}_1 \rangle = c\langle \mathcal{H}_+\hat{\Phi}_1, \hat{\Phi}_1 \rangle.$$

By the positivity of $\mathcal{H}_+$, we have $c = 0$ or $\hat{\Phi}_1 = \mathbf{0}$, i.e., $\mathcal{H}_-\boldsymbol{g} = \mathbf{0}$, which implies immediately that $\mathrm{null}(\mathcal{H}^3) \subset \mathrm{null}(\mathcal{H}^2)$. Therefore, $\mathrm{null}(\mathcal{H}^3) = \mathrm{null}(\mathcal{H}^2)$. □

2.3.2. *Without an internal atomic Josephson junction* ($\Omega = 0$)

Similar to the preceding scenario, we shall initially delineate the conditions that ensure the existence and uniqueness of the ground state solution of (1.7).

Lemma 2 (Existence and uniqueness of the ground state [7])**.** *Suppose* $V(x) \geq 0$ *satisfying* $\lim_{|x|\to\infty} V(x) = \infty$ *and at least one of the following conditions holds,*

(i) $d = 1$;
(ii) $d = 2$ *and* $\beta_{11} \geq -C_b/\alpha, \beta_{22} \geq -C_b/(1-\alpha)$, *and* $\beta_{12} = \beta_{21} \geq -\sqrt{C_b + \alpha\beta_{11}}\sqrt{C_b + (1-\alpha)\beta_{22}}$;
(iii) $d = 3$ *and* $\begin{bmatrix} \beta_{11} & \beta_{12} \\ \beta_{21} & \beta_{22} \end{bmatrix}$ *is either positive semi-definite or nonnegative,*

there exists a ground state $\Phi_g = (\phi_1^g, \phi_2^g)^\top$ *of* (1.7). *Furthermore, if the matrix* $\begin{bmatrix} \beta_{11} & \beta_{12} \\ \beta_{21} & \beta_{22} \end{bmatrix}$ *is positive semi-definite, then the ground state* $(|\phi_1^g|, |\phi_2^g|)^\top$ *is unique.*

Theorem 6 (Nullspace of $\mathcal{H}_-$ for system without JJ ($\Omega = 0$)). *Under conditions of Lemma 2, we have the following property for nullspace of $\mathcal{H}_-$*

$$\mathrm{span}\{\Phi_1, \Phi_2\} \subset \mathrm{null}(\mathcal{H}_-),$$

where $\Phi_1 = \Phi_g$, $\Phi_2 = (c_1\phi_1^g, c_2\phi_2^g)^\top$, *and* $(c_1, c_2) = \big(-(\frac{1-\alpha}{\alpha})^{1/2}, (\frac{\alpha}{1-\alpha})^{1/2}\big)$.

Proof. Noticing the fact that $\mathcal{H}_-\Phi_1 = \mathcal{H}_-\Phi_g = 0$. Actually, the operator $\mathcal{H}_-$ could be simplified below

$$\mathcal{H}_- = \begin{bmatrix} -\frac{1}{2}\nabla^2 + V(\boldsymbol{x}) + \frac{\delta}{2} + \beta_{11}|\phi_1^\alpha|^2 + \beta_{12}|\phi_2^\alpha|^2 - \mu_1 & 0 \\ 0 & -\frac{1}{2}\nabla^2 + V(\boldsymbol{x}) - \frac{\delta}{2} + \beta_{21}|\phi_1^\alpha|^2 + 2\beta_{22}|\phi_2^\alpha|^2 - \mu_2 \end{bmatrix}.$$

Then, according to Eqn. (1.9), we obtain that Φ_2 lie in the nullspace of $\mathcal{H}_-$, i.e., $\mathcal{H}_-\Phi_2 = 0$. It is easy to check that $\langle\Phi_1, \Phi_2\rangle = 0$ and $\|\Phi_2\| = 1$ with $c_1 = -(\frac{1-\alpha}{\alpha})^{1/2}$, $c_2 = (\frac{\alpha}{1-\alpha})^{1/2}$. □

Remark 3. From our extensive numerical results, not fully shown here, we conjecture that the following property holds

$$\mathcal{H}_+ \text{ is positive definite and } \mathrm{null}(\mathcal{H}_-) = \mathrm{span}\{\Phi_1, \Phi_2\}.$$

At last, we shall give the structure of the generalized nullspace of the operator $\mathcal{H}$.

Theorem 7 (Generalized nullspace of $\mathcal{H}$ for system without JJ ($\Omega = 0$)). *If the above property is true, we can obtain the generalized nullspace of $\mathcal{H}$ as follows*

$$\mathrm{null}(\mathcal{H}^3) = \mathrm{null}(\mathcal{H}^2) = \mathrm{null}(\mathcal{H}) \oplus \mathrm{span}\left\{\begin{bmatrix} \hat{\Phi}_1 \\ \mathbf{0} \end{bmatrix}, \begin{bmatrix} \hat{\Phi}_2 \\ \mathbf{0} \end{bmatrix}\right\}, \tag{2.24}$$

where $\hat{\Phi}_j = \mathcal{H}_+^{-1}\Phi_j$, $j = 1, 2$ *and* $\mathrm{null}(\mathcal{H}) = \mathrm{span}\left\{\begin{bmatrix} \mathbf{0} \\ \Phi_1 \end{bmatrix}, \begin{bmatrix} \mathbf{0} \\ \Phi_2 \end{bmatrix}\right\}$.

Proof. Similar as Theorem 5, we can prove $\mathrm{null}(\mathcal{H}) = \mathrm{span}\left\{\begin{bmatrix} \mathbf{0} \\ \Phi_1 \end{bmatrix}, \begin{bmatrix} \mathbf{0} \\ \Phi_2 \end{bmatrix}\right\}$,

$$\begin{aligned} \mathrm{null}(\mathcal{H}^2) &= \{(\boldsymbol{f}, \boldsymbol{g})^\top | \boldsymbol{g} \in \mathrm{null}(\mathcal{H}_-), \boldsymbol{f} \in \mathcal{H}_+^{-1}\mathrm{null}(\mathcal{H}_-)\} \\ &= \mathrm{null}(\mathcal{H}) \oplus \mathrm{span}\left\{\begin{bmatrix} \hat{\Phi}_1 \\ \mathbf{0} \end{bmatrix}, \begin{bmatrix} \hat{\Phi}_2 \\ \mathbf{0} \end{bmatrix}\right\}. \end{aligned}$$

Then, for $\mathrm{null}(\mathcal{H}^3)$

$$\begin{aligned} \mathrm{null}(\mathcal{H}^3) &= \{(\boldsymbol{f}, \boldsymbol{g})^\top | \mathcal{H}_-\mathcal{H}_+\mathcal{H}_-\boldsymbol{g} = \mathbf{0}, \mathcal{H}_+\mathcal{H}_-\mathcal{H}_+\boldsymbol{f} = 0\} \\ &= \{(\boldsymbol{f}, \boldsymbol{g})^\top | \mathcal{H}_-\boldsymbol{g} \in \mathcal{H}_+^{-1}\mathrm{null}(\mathcal{H}_-), \boldsymbol{f} \in \mathcal{H}_+^{-1}\mathrm{null}(\mathcal{H}_-)\}. \end{aligned}$$

Obviously, $\mathrm{null}(\mathcal{H}^2) \subset \mathrm{null}(\mathcal{H}^3)$. Then we prove that $\mathrm{null}(\mathcal{H}^3) \subset \mathrm{null}(\mathcal{H}^2)$. For any $(\boldsymbol{f}, \boldsymbol{g})^\top \in \mathrm{null}(\mathcal{H}^3)$, i.e., $\mathcal{H}_-\boldsymbol{g} \in \mathcal{H}_+^{-1}\mathrm{null}(\mathcal{H}_-)$, we have $\mathcal{H}_-\boldsymbol{g} \in \mathcal{H}_+^{-1}\mathrm{null}(\mathcal{H}_-)$, then $\mathcal{H}_-\boldsymbol{g} = c_1\hat{\Phi}_1 + c_2\hat{\Phi}_2$, and

$$\begin{aligned} 0 &= \langle\mathbf{0}, \boldsymbol{g}\rangle = \langle\mathcal{H}_-(c_1\Phi_1 + c_2\Phi_2), \boldsymbol{g}\rangle \\ &= \langle c_1\Phi_1 + c_2\Phi_2, \mathcal{H}_-\boldsymbol{g}\rangle \\ &= \langle c_1\Phi_1 + c_2\Phi_2, c_1\hat{\Phi}_1 + c_2\hat{\Phi}_2\rangle \\ &= \langle\mathcal{H}_+(c_1\hat{\Phi}_1 + c_2\hat{\Phi}_2), c_1\hat{\Phi}_1 + c_2\hat{\Phi}_2\rangle. \end{aligned}$$

Combining the positivity of $\mathcal{H}_+$, we have $c_1\hat{\Phi}_1 + c_2\hat{\Phi}_2 = \mathbf{0}$, i.e., $\mathcal{H}_-\boldsymbol{g} = \mathbf{0}$. That is to say, $\mathrm{null}(\mathcal{H}^3) \subset \mathrm{null}(\mathcal{H}^2)$, and the proof is completed. □

The convergence of the non-zero eigenvalues depends heavily on the approximation accuracy of the generalized nullspace that is associated with $\mathcal{H}$ [28]. Based on Theorems 5 and 7, we obtain the generalized nullspace of $\mathcal{H}$, thus essentially improving the convergence and efficiency.

3. Numerical method

In this section, we will propose an efficient and spectrally accurate numerical method to solve the BdG Eqs. (2.21). Due to the presence of external trapping potential $V(\boldsymbol{x})$, the ground states $\Phi_g(\boldsymbol{x})$ and eigenfunctions $(\boldsymbol{u}, \boldsymbol{v})$ are all smooth and fast-decaying. Therefore, it is reasonable to truncate the whole space $\mathbb{R}^d$ into a large enough bounded domain $D \subset \mathbb{R}^d$ with periodic boundary conditions such that the truncation error is negligible. Since all related functions are smooth, the Fourier spectral method stands out as the best candidate for spatial discretization [8,22,30] due to its simplicity, spectral accuracy and great efficiency. The computation domain is usually chosen as a rectangle $D_L := [-L, L]^d$ and discretized uniformly with N grid points in each spatial direction.

3.1. Spatial discretization by fourier spectral method

Provided that the stationary states Φ_g and all chemical potentials are precomputed with a very fine mesh by the PCG method [33], such that the numerical accuracy approaches machine precision. For simplicity, we choose to illustrate the spatial discretization for the 1D case, and extensions to higher dimensions are omitted here. We choose the computational domain $D_L := [-L, L]$ and discretize it uniformly with mesh size $h_x = \frac{2L}{N}$ where N is a positive even integer. Define the grid point set as $\mathcal{T}_N = \{(-N/2, \cdots, N/2)h_x\}$ and introduce the plane wave basis as

$$W_k(x) = e^{\mathrm{i}\mu_k(x+L)}, \quad \text{for } -N/2 \le k \le N/2-1,$$

with $\mu_k = \pi k/L$. Define $F_n := F(x_n)$ ($F = \phi_j^g, u_j, v_j, V$ etc.) as function value at grid point $x_n \in \mathcal{T}_N$ and $\mathbf{F} = (F_1, F_2, \dots, F_N)$ as the corresponding discrete vector. The FS approximations of F, denoted by $\widetilde{F}$, and its Laplacian $\nabla^2 F$ read as follows

$$F(x) \approx \widetilde{F}(x) := \sum_{k=-M/2}^{M/2-1} \widehat{\mathbf{F}}_k \, W_k(x), \quad (\nabla^2 F)(x) \approx (\nabla^2 \widetilde{F})(x) = \sum_{k=-N/2}^{N/2-1} -\mu_k^2 \, \widehat{\mathbf{F}}_k \, W_k(x), \tag{3.1}$$

where $\widehat{\mathbf{F}}_k$, the discrete Fourier transform of vector $\mathbf{F} \in \mathbb{C}^N$, is computed as

$$\widehat{\mathbf{F}}_k = \frac{1}{N} \sum_{n=0}^{N-1} F_n \overline{W}_k(x_n) = \frac{1}{N} \sum_{n=0}^{N-1} F_n \, e^{\frac{-\mathrm{i}2\pi nk}{N}}, \qquad -N/2 \le k \le N/2-1, \tag{3.2}$$

and is accelerated by a discrete Fast Fourier Transform (FFT) within $O(N \ln(N))$ float operations. The numerical approximation of the Laplacian operator ∇^2, denoted as $[\![\nabla^2]\!]$, corresponds to a dense matrix [22,25,36]. We map the function's pointwise multiplication $F_n G_n$ as a matrix-vector product $[\![F]\!]\mathbf{G}$, that is,

$$([\![F]\!]\mathbf{G})_n := F_n G_n \quad \Longrightarrow \quad [\![F]\!] = \mathrm{diag}(\mathbf{F}). \tag{3.3}$$

The operators L_1, L_2 in (2.5) is then discretized as follows

$$[\![L_1]\!] = -\frac{1}{2}[\![\nabla^2]\!] + [\![V]\!] + \frac{\delta}{2} + 2\beta_{11}[\![|\phi_1^g|^2]\!] + \beta_{12}[\![|\phi_2^g|^2]\!] - \mu_g,$$
$$[\![L_2]\!] = -\frac{1}{2}[\![\nabla^2]\!] + [\![V]\!] - \frac{\delta}{2} + \beta_{21}[\![|\phi_1^g|^2]\!] + 2\beta_{22}[\![|\phi_2^g|^2]\!] - \mu_g.$$

Therefore, operators $\mathcal{A}$ and $\mathcal{B}$ are mapped into matrices $\mathbf{A}$ and $\mathbf{B}$ in the following way

$$\mathbf{A} := \begin{bmatrix} [\![L_1]\!] & \beta_{12}[\![\phi_1^g \phi_2^g]\!] + \frac{\Omega}{2} \\ \beta_{21}[\![\phi_1^g \phi_2^g]\!] + \frac{\Omega}{2} & [\![L_2]\!] \end{bmatrix}, \quad \mathbf{B} := \begin{bmatrix} \beta_{11}[\![|\phi_1^g|^2]\!] & \beta_{12}[\![\phi_1^g \phi_2^g]\!] \\ \beta_{21}[\![\phi_1^g \phi_2^g]\!] & \beta_{22}[\![|\phi_2^g|^2]\!] \end{bmatrix}. \tag{3.4}$$

Thanks to the Fourier spectral discretization, both matrices $\mathbf{A}$ and $\mathbf{B}$ are symmetric, thus keeping their continuous operators' Hermitian property. Setting $\boldsymbol{u}_N = (\boldsymbol{u}_1^N; \boldsymbol{u}_2^N)$ and $\boldsymbol{v}_N = (\boldsymbol{v}_1^N; \boldsymbol{v}_2^N)$, the BdG Eqs. (2.20) with constaint (2.4) are then discretized into a linear eigenvalue problem

$$\begin{bmatrix} \mathbf{A} & \mathbf{B} \\ -\mathbf{B} & -\mathbf{A} \end{bmatrix} \begin{bmatrix} \boldsymbol{u}_N \\ \boldsymbol{v}_N \end{bmatrix} = \omega_N \begin{bmatrix} \boldsymbol{u}_N \\ \boldsymbol{v}_N \end{bmatrix}, \quad h_x \left(\|\boldsymbol{u}_N\|_{l^2}^2 - \|\boldsymbol{v}_N\|_{l^2}^2 \right) = 1. \tag{3.5}$$

With a similar change of variables, i.e., $\boldsymbol{f}_N = \frac{1}{2}(\boldsymbol{u}_N + \boldsymbol{v}_N)$, $\boldsymbol{g}_N = \frac{1}{2}(\boldsymbol{u}_N - \boldsymbol{v}_N)$, the above equation is rewritten into a linear response eigenvalue problem

$$\begin{bmatrix} \mathbf{H}_+ & \mathbf{O} \\ \mathbf{O} & \mathbf{H}_- \end{bmatrix} \begin{bmatrix} \boldsymbol{f}_N \\ \boldsymbol{g}_N \end{bmatrix} = \omega_N \begin{bmatrix} \mathbf{O} & \mathbf{I} \\ \mathbf{I} & \mathbf{O} \end{bmatrix} \begin{bmatrix} \boldsymbol{f}_N \\ \boldsymbol{g}_N \end{bmatrix}, \tag{3.6}$$

where $\mathbf{H}_+ = \mathbf{A} + \mathbf{B}$, $\mathbf{H}_- = \mathbf{A} - \mathbf{B}$. The above discrete dense eigensystem is solved using the recently developed Bi-Orthogonal Structure Preserving algorithm (BOSP for short) [28], and details are illustrated in the coming subsection.

3.2. A bi-orthogonal structure-preserving method

As is known that ARPACK is a standard library to compute the discrete eigenvalue and eigenvector problem, and it has been successfully adapted to BdG equations of dipolar BEC [19,22]. However, a similar adaptation attempt using ARPACK is not as effective, and sometimes it does not even converge within a reasonable time, because the generalized nullspace is much larger and more complicated, not to even mention the large-scale dense eigensystem for three-dimensional problems. It is worth pointing out that the eigenspaces associated with eigenvalues of different magnitudes are bi-orthogonal to each other, and such bi-orthogonal property shall be taken into account in the eigensolver design [23,24,28] so as to achieve better performance. The structure of generalized nullspace and bi-orthogonal, well described in Section 2 on the continuous level, are assessed numerically by the linear algebra package (LAPACK) and a modified Gram-Schmidt bi-orthogonal algorithm.

Based on the recently developed linear response eigensolver BOSP [28], by combining the Fourier spectral method for spatial approximation and making use of the specific generalized nullspace structure (Section 2.3), we propose an efficient iterative subspace eigensolver and provide a friendly interface for matrix-vector product evaluation. Since there is no explicit matrix storage and the

matrix-vector product is implemented via FFT within almost optimal $O(N_t \log N_t)$ operations ($N_t := N^d$ is the total number of grid points), the heavy memory burden is much more alleviated and the computational efficiency is guaranteed to a large extent. Therefore, it provides a feasible solution to large-scale problems, especially for such a densely populated eigensystem. Thanks to the Fourier spectral method, our method can achieve spectral accuracy for both eigenvalues and eigenvectors as long as the accuracy tolerance of BOSP is chosen sufficiently small.

As pointed out earlier, the matrix-vector product evaluation is the most time-consuming part. While in this article, the matrix-vector product

$$\mathbf{H}_+ \boldsymbol{f}_N, \quad \mathbf{H}_- \boldsymbol{g}_N, \quad \text{for} \quad \boldsymbol{f}_N, \boldsymbol{g}_N \in \mathbb{R}^{2N_t}, \tag{3.7}$$

can be realized by two pairs of FFT/iFFT plus some function multiplication in the physical space. The overall computational costs to compute the first $n_e \in \mathbb{Z}^+$ eigenpairs amounts to

$$\mathcal{O}(n_e) \times \left(\mathcal{O}(N_t \log(N_t)) + \mathcal{O}(N^d)\right) + \mathcal{O}(n_e^3) = \mathcal{O}(n_e\ N_t \log(N_t)) + \mathcal{O}(n_e^3).$$

When the degree of freedom is much larger than the number of eigenvalues, i.e., $N_t \gg n_e$, the computational costs are approximately $\mathcal{O}(N_t \log(N_t))$ and will be verified numerically in the next section.

Remark 4 (Extension to complex-valued BdG system)**.** Our proposed method is efficient and effective for real-valued BdG systems. While for complex-valued BdG systems (for example, BdG of the rotating BEC with complex-valued ground state), direct extension is impractical and one has to first transform the original complex-valued system into real-valued linear response problem. We shall report results on this topic in a forthcoming work [37].

3.3. Stability analysis and error estimates

To demonstrate the practicality of our solver, we will present a rigorous stability analysis for the eigenfunctions in this subsection. Since the density and eigenfunction both decay fast enough in space, it is reasonable to assume that $q(\boldsymbol{x})$ ($q = \phi_j^g, u_j, v_j$, etc.) is numerically compactly supported in a bounded domain $\Omega \subsetneq \mathbb{R}^d$, that is, $\mathrm{supp}\{q\} \subsetneq \Omega$. We introduce $2L$-periodic Sobolev space $H_p^m(\Omega) \subset H^m(\Omega)$ $(m \geq 1)$ with $\Omega = D_L$, and the semi-norm and norm as follows, respectively,

$$|q|_m := \left(\sum\nolimits_{|\boldsymbol{\alpha}|=m} \|\partial^{\boldsymbol{\alpha}} q\|^2\right)^{1/2}, \quad \|q\|_m := \left(\sum\nolimits_{|\boldsymbol{\alpha}|\leq m} \|\partial^{\boldsymbol{\alpha}} q\|^2\right)^{1/2},$$

with index $\boldsymbol{\alpha} = (\alpha_1, \ldots, \alpha_d) \in \mathbb{Z}^d$, $|\boldsymbol{\alpha}| = \sum_{j=1}^d \alpha_j$, $\partial^{\boldsymbol{\alpha}} = \partial_{x_1}^{\alpha_1} \cdots \partial_{x_d}^{\alpha_d}$ and $\|\cdot\|$ being the L^2 norm. For vector-valued function $\boldsymbol{q} = (q_1, q_2)^\top$, we define $|\boldsymbol{q}|_m := \sqrt{\sum_j |q_j|_m^2}$, $\|\boldsymbol{q}\|_m := \sqrt{\sum_j \|q_j\|_m^2}$, and $\|\boldsymbol{q}\| := \sqrt{\sum_j \|q_j\|^2}$. We use $A \lesssim B$ to denote $A \leq cB$ where the constant $c > 0$ is independent of N. Then we first introduce the stability analysis as follows:

Theorem 8 (Stability Analysis)**.** *For any $\boldsymbol{q}(\boldsymbol{x}) = (q_1(\boldsymbol{x}), q_2(\boldsymbol{x}))^\top \in (H_p^m(\Omega))^2$ with $m > d/2 + 2$, and its Fourier spectral approximations $\widetilde{\boldsymbol{q}}(\boldsymbol{x}) = \left(\widetilde{q}_1(\boldsymbol{x}), \widetilde{q}_2(\boldsymbol{x})\right)^\top$, we have the following error estimate*

$$\|\mathcal{Q}\boldsymbol{q} - \mathcal{Q}\widetilde{\boldsymbol{q}}\| \lesssim N^{-(m-2)}, \tag{3.8}$$

where $\mathcal{Q} = \mathcal{A}, \mathcal{B}$, and $\boldsymbol{q} = \boldsymbol{u}, \boldsymbol{v}$.

To prove the above theorem, the following preparations are required.

Lemma 3 (Fourier spectral approximation [36,38])**.** *For $q(\boldsymbol{x}) \in H_p^m(\Omega)$ with $m > d/2$, and its Fourier spectral approximation $\mathcal{I}_N q$, we have the following error estimates*

$$\|\partial^{\boldsymbol{\alpha}}(q - \widetilde{q})\| \lesssim N^{-(m-|\boldsymbol{\alpha}|)} |q|_m, \qquad 0 \leq |\boldsymbol{\alpha}| \leq m. \tag{3.9}$$

Since operators $\mathcal{A}$ and $\mathcal{B}$ contain only two types of operators, namely, the Laplacian operator ∇^2 and function multiplication operation that involves $V(\boldsymbol{x})$ & $\phi_i^g \phi_j^g$, the following corollary is a prerequisite for proving Theorem 8.

Corollary 1. *For $q(\boldsymbol{x}) \in H_p^m(\Omega)$ with $m > d/2$, and its Fourier spectral approximation $\mathcal{I}_N q$, we have*

$$\|\nabla^2 q - \nabla^2 \widetilde{q}\| \lesssim N^{-(m-2)} |q|_m, \tag{3.10}$$

$$\|Vq - V\widetilde{q}\| \lesssim N^{-m} |q|_m, \tag{3.11}$$

$$\|\phi_j^g \phi_l^g q - \phi_j^g \phi_l^g \widetilde{q}\| \lesssim N^{-m} |q|_m \quad (j, l = 1, 2). \tag{3.12}$$

It is easy to prove the above corollary using Lemma 3, and we shall omit details for brevity.

The proof of Theorem 8:

Proof. For simplicity, we only prove the $\mathcal{Q} = \mathcal{A}$ case and extensions to other operators are similar. From (2.5) and (3.9)-(3.11), we obtain

$$\|(-1/2\nabla^2)\mathbf{I}_2(\boldsymbol{q}) - (-1/2\nabla^2)\mathbf{I}_2(\widetilde{\boldsymbol{q}})\| \lesssim N^{-(m-2)} |\boldsymbol{q}|_m,$$

where $\mathbf{I}_2$ is the second-order unit diagonal matrix.

For the other term of $\mathcal{A}$ as shown in Eq. (2.5), using Eq. (3.9), Eq. (3.12) and triangle inequality, the following error estimate holds:

$$\left\|\left(\mathcal{A}-(-1/2\nabla^2)\mathbf{I}_2\right)\boldsymbol{q}-\left(\mathcal{A}-(-1/2\nabla^2)\mathbf{I}_2\right)\widetilde{\boldsymbol{q}}\right\| \lesssim N^{-m}|\boldsymbol{q}|_m.$$

Therefore, we finish the proof of Theorem 8. □

Then we will propose the error estimates for the FS approximations. To begin with, and adopt the Sobolev space $\mathbb{V}=(H_p^1(\Omega))^2\times(H_p^1(\Omega))^2$ with the following norm

$$\|\boldsymbol{\Phi}\|_1=\sqrt{\|\boldsymbol{f}\|_1^2+\|\boldsymbol{g}\|_1^2}\quad\text{and}\quad\|\boldsymbol{\Phi}\|=\sqrt{\|\boldsymbol{f}\|^2+\|\boldsymbol{g}\|^2},\qquad\forall\boldsymbol{\Phi}:=(\boldsymbol{f};\boldsymbol{g})\in\mathbb{V}.$$

The BdG Eq. (2.21) is equivalent to the following eigenvalue problem:

$$\widetilde{\mathcal{H}}\begin{bmatrix}\boldsymbol{f}\\ \boldsymbol{g}\end{bmatrix}:=\begin{bmatrix}\mathcal{H}_+ & \mathcal{O}\\ \mathcal{O} & \mathcal{H}_-\end{bmatrix}\begin{bmatrix}\boldsymbol{f}\\ \boldsymbol{g}\end{bmatrix}=\omega\begin{bmatrix}0 & 1\\ 1 & 0\end{bmatrix}\begin{bmatrix}\boldsymbol{f}\\ \boldsymbol{g}\end{bmatrix}=:\omega\mathcal{J}\begin{bmatrix}\boldsymbol{f}\\ \boldsymbol{g}\end{bmatrix}. \tag{3.13}$$

The Galerkin weak form of Eq. (3.13) reads as: to find $0\neq\omega\in\mathbb{R}$ and $\boldsymbol{\Phi}=(\boldsymbol{f};\boldsymbol{g})\in\mathbb{V}$ such that

$$a(\boldsymbol{\Phi},\boldsymbol{\Psi})=\omega\, b(\boldsymbol{\Phi},\boldsymbol{\Psi}),\quad\forall\boldsymbol{\Psi}=(\boldsymbol{\xi};\boldsymbol{\eta})\in\mathbb{V}, \tag{3.14}$$

subject to constraint $b(\boldsymbol{\Phi},\boldsymbol{\Phi})=1/2$ with

$$a(\boldsymbol{\Phi},\boldsymbol{\Psi}):=\left\langle\mathcal{H}_+\boldsymbol{f},\boldsymbol{\xi}\right\rangle+\langle\mathcal{H}_-\boldsymbol{g},\boldsymbol{\eta}\rangle,\quad b(\boldsymbol{\Phi},\boldsymbol{\Psi}):=\langle\boldsymbol{g},\boldsymbol{\xi}\rangle+\langle\boldsymbol{f},\boldsymbol{\eta}\rangle.$$

Remark 5. From Remark 2 (or 3), we can prove that there exists $c_0>0$ such that

$$a(\boldsymbol{\Phi},\boldsymbol{\Phi})\geq c_0\|\boldsymbol{\Phi}\|_1,\quad\forall\boldsymbol{\Phi}\in\mathbb{U}, \tag{3.15}$$

where the subspace $\mathbb{U}$ is defined as

$$\mathbb{U}=\mathrm{null}(\mathcal{H}_+)^\perp\times\mathrm{null}(\mathcal{H}_-)^\perp\subset\mathbb{V},$$

with $\mathrm{null}(\mathcal{H}_\pm)^\perp:=\{\boldsymbol{f}\in(H_p^1(\Omega))^2\,|\,\langle\boldsymbol{f},\boldsymbol{\xi}\rangle=0,\ \forall\boldsymbol{\xi}\in\mathrm{null}(\mathcal{H}_\pm)\}$. It is important to point out that solving the BdG Eq. (3.14) in $\mathbb{U}$ is equivalent to solving non-zero ω and its associated eigenfunction $\boldsymbol{\Phi}$ in $\mathbb{V}$.

Define the approximation finite dimensional spaces X_N of $H_p^1(\Omega)$ and $\mathbb{V}_N$ of $\mathbb{V}$ as follows:

$$X_N:=\mathrm{span}\left\{W_k(\boldsymbol{x}),k=-N/2,\dots,N/2-1\right\},\quad\mathbb{V}_N:=(X_N)^2\times(X_N)^2,$$

and consider its approximation problem: to find $0\neq\omega_N\in\mathbb{R}$ and $\boldsymbol{\Phi}_N=(\boldsymbol{f}_N;\boldsymbol{g}_N)\in\mathbb{V}_N$ such that

$$a_N(\boldsymbol{\Phi}_N,\boldsymbol{\Psi}_N)=\omega_N\, b_N(\boldsymbol{\Phi}_N,\boldsymbol{\Psi}_N),\quad\forall\boldsymbol{\Psi}_N=(\boldsymbol{\xi}_N;\boldsymbol{\eta}_N)\in\mathbb{V}_N, \tag{3.16}$$

subject to normalization constraint $b_N(\boldsymbol{\Phi}_N,\boldsymbol{\Phi}_N)=1/2$ with

$$a_N(\boldsymbol{\Phi}_N,\boldsymbol{\Psi}_N)=\left\langle\mathcal{H}_+\boldsymbol{f}_N,\boldsymbol{\xi}_N\right\rangle_N+\langle\mathcal{H}_-\boldsymbol{g}_N,\boldsymbol{\eta}_N\rangle_N,\quad b_N(\boldsymbol{\Phi}_N,\boldsymbol{\Psi}_N)=\langle\boldsymbol{g}_N,\boldsymbol{\xi}_N\rangle_N+\langle\boldsymbol{f}_N,\boldsymbol{\eta}_N\rangle_N,$$

and $\langle\boldsymbol{f},\boldsymbol{\xi}\rangle_N:=\sum_j\left\langle f_j^N,\xi_j^N\right\rangle_N:=\sum_j\left(\frac{2L}{N}\sum_{n=0}^N f_j^N(\boldsymbol{x}_n)\overline{g_j^N(\boldsymbol{x}_n)}\right)$.

Similar to [29, Lemma A.1], we have the following equivalence result and choose to omit proofs for brevity.

Lemma 4. *The discrete problem (3.6) and the discrete variational problem (3.16) are equivalent.*

To illustrate the convergence behavior, we introduce the following notation

$$\delta_N(\boldsymbol{\Phi})=\inf_{\boldsymbol{\Psi}\in\mathbb{V}_N}\left\{\|\boldsymbol{\Phi}-\boldsymbol{\Psi}\|_1+\sup_{\boldsymbol{\Theta}\in\mathbb{V}_N}\frac{|a(\boldsymbol{\Psi},\boldsymbol{\Theta})-a_N(\boldsymbol{\Psi},\boldsymbol{\Theta})|}{\|\boldsymbol{\Theta}\|_1}\right\}. \tag{3.17}$$

Similar as [29, Lemma A. 2] for scalar function, by the coerciveness of bilinear operator $a(\cdot,\cdot)$ (Eq. (3.15)) and the conformal subspace approximation, we obtain

$$\delta_N(\boldsymbol{\Phi})\lesssim N^{-(m-\sigma)},\qquad\text{with}\quad\sigma=\max\{1,d/2\}. \tag{3.18}$$

According to the general theory given by [29, Lemma A. 3], we derive the following error estimates.

Lemma 5. *For any eigenpair approximation $\{\omega_N;\boldsymbol{\Phi}_N\}$ of Eq. (3.16), there is an eigenpair $\{\omega;\boldsymbol{\Phi}\}$ of Eq. (3.14) corresponding to ω such that*

$$\|\boldsymbol{\Phi}-\boldsymbol{\Phi}_N\|_1\lesssim\delta_N(\boldsymbol{\Phi}),\quad\|\boldsymbol{\Phi}-\boldsymbol{\Phi}_N\|\lesssim\zeta_N\|\boldsymbol{\Phi}-\boldsymbol{\Phi}_N\|_1,\quad|\omega-\omega_N|\lesssim\|\boldsymbol{\Phi}-\boldsymbol{\Phi}_N\|_1^2,$$

where the constant ζ_N approaches 0 as $N\to\infty$.

Finally, via a change of variables, we obtain error estimates for $(\boldsymbol{u},\boldsymbol{v})$.

Theorem 9 (Error Estimates). *If $\boldsymbol{u},\boldsymbol{v}\in(H_p^m(\Omega))^2$ with $m\geq1$ and $\mathrm{supp}\{\boldsymbol{u}\},\mathrm{supp}\{\boldsymbol{v}\}\subsetneq\Omega$, then for any eigenpair approximation $\{\omega_N;\boldsymbol{u}_N,\boldsymbol{v}_N\}$ of (3.5), there is an eigenpair $\{\omega;\boldsymbol{u},\boldsymbol{v}\}$ of Eq. (2.20) satisfying the following error estimates*

$$\|\boldsymbol{u}-\boldsymbol{u}_N\|+\|\boldsymbol{v}-\boldsymbol{v}_N\|\lesssim N^{-(m-\sigma)},$$
$$|\omega-\omega_N|\lesssim N^{-2(m-\sigma)},$$

where $\sigma=\max\{1,d/2\}$.

Table 1
Errors of the eigenvalue/eigenvector for **Case I** in **1D** for with/without **JJ** in Example 1.

	N	32	64	128	256	512
$\Omega = 1$	E^x_ω	1.917E-02	4.786E-06	1.490E-10	4.441E-15	7.994E-15
	$\mathrm{E}^x_{\boldsymbol{uv}}$	3.660E-02	1.077E-03	4.103E-07	9.817E-12	1.948E-11
$\Omega = 0$	E^x_ω	8.391E-02	2.398E-06	1.461E-10	4.249E-12	1.827E-13
	$\mathrm{E}^x_{\boldsymbol{uv}}$	1.728	1.077E-03	1.461E-07	1.675E-10	1.997E-11

4. Numerical results

In this section, we shall first carry out a comprehensive numerical investigation to illustrate the accuracy and efficiency. Then we apply our method to study the Bogoliubov excitations around the ground states. The ground states Φ_g and its associated chemical potentials are computed with a very fine mesh size on a large enough domain using the PCG method, thus achieving an up to almost machine-precision accuracy. Unless stated otherwise, we choose harmonic trapping potential $V(\boldsymbol{x})$ as described in (1.2) and denote the trapping frequencies by a vector $\vec{\boldsymbol{\gamma}} \in \mathbb{R}^d$, for example, $\vec{\boldsymbol{\gamma}} = (1, 2, 3)$ represents $\gamma_x = 1, \gamma_y = 2, \gamma_z = 3$ for 3D harmonic trap. The computation domain is chosen as a rectangular $\mathcal{D}_L = [-L, L]^d$ and discretized uniformly with the same $N \in 2\mathbb{Z}^+$ grid points in each spatial direction. The mesh sizes are chosen the same in each direction and denoted as h for simplicity. Throughout this section, we shall take $L = 16$ for the 1D and 2D problems and $L = 8$ in the 3D computation.

The relative error of the eigenvalue is expected to satisfy a prescribed tolerance of 10^{-9} throughout this section. We shall compute BdG excitations of CGPEs (1.1a)-(1.1b) with Josephson junctions (**JJ**) (i.e., $\Omega = 1$ and $\delta = 0$) and without Josephson junctions (i.e., $\Omega = 0, \delta = 0$ and $\alpha = 0.2$) where the interaction strength coefficients are chosen as $\beta_{11} = 100, \beta_{12} = 94, \beta_{22} = 97$. The algorithms were implemented in Fortran (ifort version 2021.3.0) and run on a 3.00 GHz Intel(R) Xeon(R) Gold 6248R CPU with a 36 MB cache in Ubuntu GNU/Linux.

4.1. Performance investigation

In this subsection, we study the performance in terms of accuracy and efficiency in different space dimensions. Analytical eigenvalues and eigenvectors were given for the harmonic trapping potential by Eq. (2.13) in Theorem 2. For an eigenvalue ω with multiplicity K, we denote its associated analytical eigenspaces as $\mathcal{M}_{\boldsymbol{u}} := \mathrm{span}\{\boldsymbol{u}_1, \cdots, \boldsymbol{u}_K\}, \mathcal{M}_{\boldsymbol{v}} := \mathrm{span}\{\boldsymbol{v}_1, \cdots, \boldsymbol{v}_K\}$. The numerical approximations of $\{\omega_\sigma; \boldsymbol{u}_\sigma, \boldsymbol{v}_\sigma\}$ are denoted by $\{\omega^N_\sigma; \boldsymbol{u}^N_\sigma, \boldsymbol{v}^N_\sigma\}$ with $\sigma \in \{x, y, z\}$. To demonstrate the results, we adopt the following error functions

$$\mathrm{E}^\sigma_\omega := \frac{|\omega^N_\sigma - \omega_\sigma|}{|\omega_\sigma|}, \qquad \mathrm{E}^\sigma_{\boldsymbol{uv}} := \frac{\|\boldsymbol{u}^N_\sigma - \mathcal{P}^N_{\boldsymbol{u}} \boldsymbol{u}^N_\sigma\|_{l^2}}{\|\boldsymbol{u}^N_\sigma\|_{l^2}} + \frac{\|\boldsymbol{v}^N_\sigma - \mathcal{P}^N_{\boldsymbol{v}} \boldsymbol{v}^N_\sigma\|_{l^2}}{\|\boldsymbol{v}^N_\sigma\|_{l^2}}, \tag{4.1}$$

where $\|\cdot\|_{l^2}$ is the discrete l^2 norm and $\mathcal{P}^N_\nu$ $(\nu = \boldsymbol{u}, \boldsymbol{v})$ is the l^2-orthogonal projection operator into space $\mathcal{M}^N_\nu$ which is the discrete version of $\mathcal{M}_\nu$ at mesh grid $\mathcal{T}_N$.

Example 1 (Accuracy)**.** We study the accuracy behavior for BdG Eq. (2.3) and Eq. (2.10) (with/without **JJ**) in 1D/2D/3D, respectively. To this end, we consider the following four cases:

Case I. 1D case: $\gamma_x = 1$;
Case II. Isotropic trap in 2D: $\gamma_x = \gamma_y = 1$;
Case III. Anisotropic trap in 2D: $\gamma_x = \gamma_y/2 = 1$;
Case IV. Isotropic trap in 3D: $\gamma_x = \gamma_y = \gamma_z = 1$.

As proved in Lemma 2, there exist d-pairs of analytical eigenvalue/vectors in d-dimensional problems for all cases and the multiplicity of eigenvalues for isotropic trap (i.e., **Case II and IV**) is d. Tables 1–3 present the numerical errors of eigenvalues and eigenvectors that are obtained with different mesh sizes in **Case I-IV**. We can observe that: (1) the numerical solutions manifest a typical spectral convergence for both eigenvalue and eigenvector; (2) the approximation errors saturate as the mesh size tends smaller and the saturated accuracy is well below the preset tolerance (10^{-9}) of our eigenvalue solver, including both the 2D and 3D problem (i.e., **Case II-IV**).

Example 2 (Efficiency)**.** We investigate the efficiency performance by computing the first 20 positive eigenvalues and the corresponding eigenfunctions with/without Josephson junction in 3D. To this end, we consider the following cases

Case I. With **JJ** for isotropic trap with $\vec{\boldsymbol{\gamma}} = (1, 1, 1)$ and anisotropic trap with $\vec{\boldsymbol{\gamma}} = (1, 1, 2)$;
Case II. Without **JJ** for isotropic trap with $\vec{\boldsymbol{\gamma}} = (1, 1, 1)$ and anisotropic trap with $\vec{\boldsymbol{\gamma}} = (1, 1, 2)$.

Table 2
Errors of the eigenvalue/eigenvector for **Case II** (upper) and **III** (lower) in **2D** with/without **JJ** in Example 1.

Case II: isotropic trap ($\gamma_x = \gamma_y = 1$)						
	N	32	64	128	256	512
$\Omega = 1$	E_ω^x	1.007E-02	1.742E-06	9.452E-13	1.028E-13	3.786E-13
	E_ω^y	1.007E-02	1.742E-06	9.484E-13	1.223E-13	3.901E-13
	E_{uv}^x	6.403E-02	7.560E-04	4.747E-08	9.157E-11	3.626E-11
	E_{uv}^y	5.525E-02	6.239E-04	3.825E-08	4.187E-11	4.246E-11
$\Omega = 0$	E_ω^x	1.007E-02	1.765E-06	9.137E-13	2.620E-14	1.914E-13
	E_ω^y	1.007E-02	1.765E-04	9.526E-13	3.086E-14	2.041E-13
	E_{uv}^x	5.910E-02	6.697E-04	6.493E-08	5.445E-12	1.590E-11
	E_{uv}^y	5.131E-02	5.470E-04	5.261E-08	2.671E-12	3.810E-11
Case III: anisotropic trap ($\gamma_x = 1, \gamma_y = 2$)						
	N	32	64	128	256	512
$\Omega = 1$	E_ω^x	7.184E-03	8.939E-06	1.954E-13	2.887E-14	3.124E-13
	E_ω^y	1.152E-02	5.077E-04	1.133E-08	2.442E-15	1.981E-13
	E_{uv}^x	4.331E-02	7.871E-04	1.191E-07	8.814E-12	1.913E-12
	E_{uv}^y	2.659E-02	9.205E-03	1.118E-05	1.391E-11	2.451E-12
$\Omega = 0$	E_ω^x	7.177E-03	8.964E-06	1.936E-13	7.771E-14	1.352E-13
	E_ω^y	1.149E-02	5.084E-04	1.132E-08	5.240E-13	8.970E-14
	E_{uv}^x	4.421E-02	7.876E-04	1.190E-07	7.059E-12	1.954E-11
	E_{uv}^y	2.658E-01	9.206E-03	1.118E-05	1.915E-11	5.950E-12

Table 3
Errors of the eigenvalue/eigenvector for **Case IV** in **3D** with/without **JJ** in Example 1.

	N	16	32	64	128
$\Omega = 1$	E_ω^x	5.883E-03	2.880E-06	2.089E-13	1.060E-12
	E_ω^y	5.883E-03	2.880E-06	2.103E-13	1.062E-12
	E_ω^z	5.883E-03	2.880E-06	2.107E-13	1.064E-12
	E_{uv}^x	7.270E-02	5.609E-04	2.575E-08	8.528E-11
	E_{uv}^y	7.275E-02	5.608E-04	2.575E-08	4.695E-11
	E_{uv}^z	7.271E-02	5.608E-04	2.575E-08	4.120E-11
$\Omega = 0$	E_ω^x	5.895E-03	2.881E-06	5.730E-13	1.798E-12
	E_ω^y	5.895E-03	2.881E-06	5.798E-13	1.811E-12
	E_ω^z	5.895E-03	2.881E-06	5.802E-13	1.820E-12
	E_{uv}^x	7.273E-02	5.610E-04	2.572E-08	1.086E-11
	E_{uv}^y	7.269E-02	5.610E-04	2.572E-08	1.372E-11
	E_{uv}^z	7.273E-02	5.610E-04	2.572E-08	1.680E-11

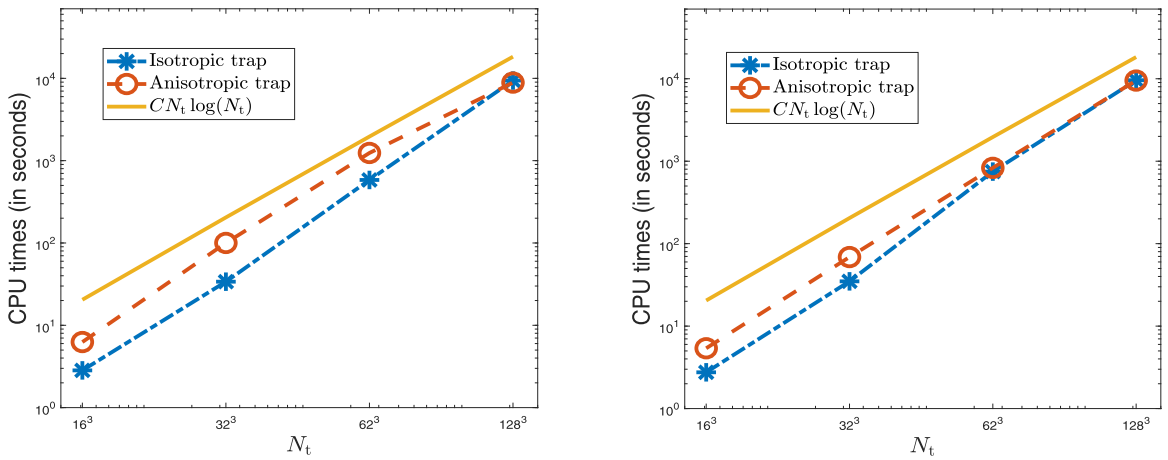

Fig. 1. The computational time versus degrees of freedom for **Case I** (left) and **Case II** (right) in Example 2.

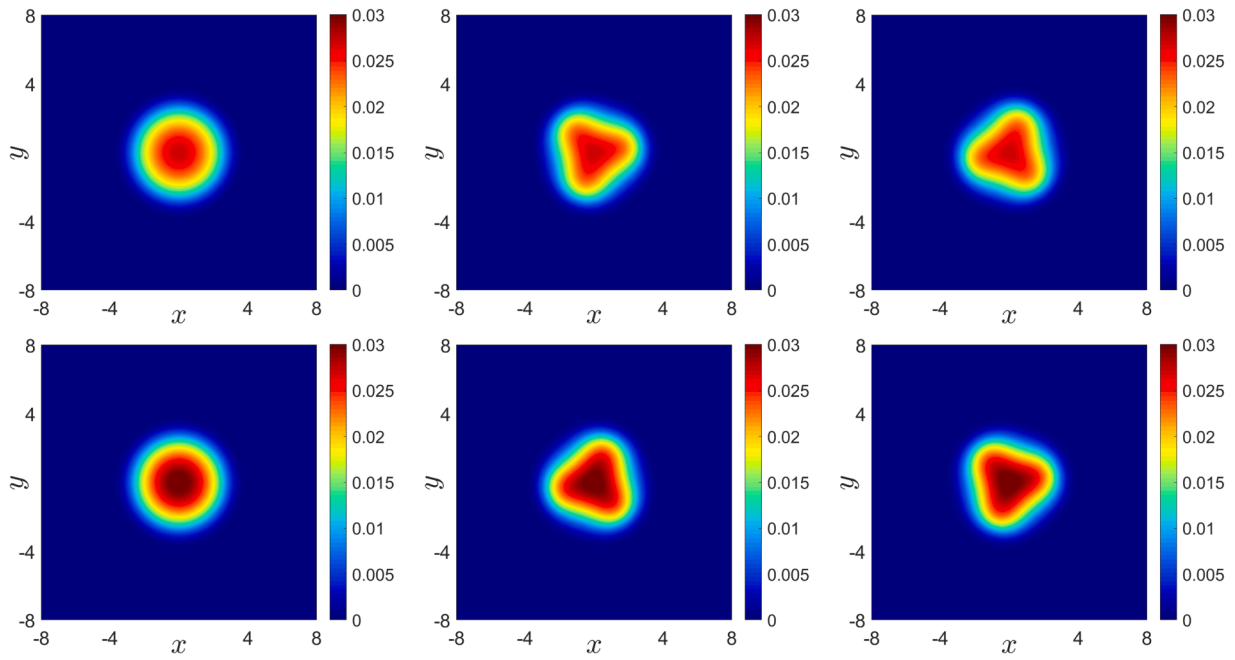

Fig. 2. Snapshots of the ground states $|\phi_j(\boldsymbol{x})|^2$ (left), perturbed densities $n_j^{\ell}(\boldsymbol{x}, t = 7.4)$ (middle) and $n_j^{\ell}(\boldsymbol{x}, t = 9.2)$ (right) by excitation mode indexed $\ell = 15$ for **Case I** in Example 3 ($j = 1$ (top), 2 (bottom)).

Fig. 1 presents the computation time (measured in seconds) versus degrees of freedom for 3D problems as described above in Example 2. The degree of freedom varies as 16 384, 131 072, 1 048 576, 8 388 608, while the number of eigenvalue is kept unchanged as $n_{\text{ev}} = 20$ with a tolerance 10^{-9}. From Fig. 1, we can see clearly that the degree of freedom is much larger than the number of desired eigenvalues, and the overall computation time scales as $\mathcal{O}(N_{\text{t}} \log N_{\text{t}})$, which agrees well with the complexity of matrix-vector multiplication as expected. Given the fact that the discrete BdG system is non-Hermitian and dense, and the first 20 eigenpairs are computed with 8 million degrees of freedom within 3 hours using sequential CPU computing, it manifests a very promising potential in physical applications.

4.2. Applications of 2D cases

In this subsection, we to investigate the excitation spectrum and Bogoliubov amplitudes of two-component BEC around the ground state. To visualize a normal mode, similar to (2.1), we analyze the evolution of the perturbed density profile [34]

$$n_j^{\ell}(\boldsymbol{x}, t) = \left| \left[\phi_j(\boldsymbol{x}) + \varepsilon \left(u_j^{\ell}(\boldsymbol{x}) e^{-i\omega_{\ell} t} + \bar{v}_j^{\ell}(\boldsymbol{x}) e^{i\omega_{\ell} t} \right) \right] \right|^2, \quad j = 1, 2, \tag{4.2}$$

which reveals the nature of excitations indexed ℓ. To this end, we use a very fine mesh size $h = 1/8$.

Example 3. We investigate the perturbed density evolution by different excitation modes with/without a Josephson junction in 2D. To this end, we set perturbation strength $\varepsilon = 0.1$ and consider the following four cases:

Case I. Isotropic trap with **JJ**: $\Omega = 1$, $\gamma_x = \gamma_y = 1$, $\ell = 15$;
Case II. Anisotropic trap with **JJ**: $\Omega = 1$, $\gamma_x = \gamma_y/2 = 1$, $\ell = 12$;
Case III. Isotropic trap without **JJ**: $\Omega = 0$, $\gamma_x = \gamma_y = 1$, $\ell = 14$;
Case IV. Anisotropic trap without **JJ**: $\Omega = 0$, $\gamma_x = \gamma_y/2 = 1$, $\ell = 16$.

Figs. 2–5 display the perturbed density evolution $n_j^{\ell}(\boldsymbol{x}, t)$ that are associated with eigenvalues ω_{ℓ} and Bogoliubov amplitudes u_j^{ℓ}, v_j^{ℓ} for **Case I–IV** in Example 3, respectively. These figures show that the Josephson junction and external potential affect the shape of the perturbed density. The perturbed densities are point/line-symmetric in a symmetric or antisymmetric external potential, respectively. Meanwhile, the perturbed density will be compressed along the direction with a larger trapping frequency. As depicted in the figures, the presence of Josephson junction brings in many more rich physical phenomena for the BdG equations, which will be detailed in the future.

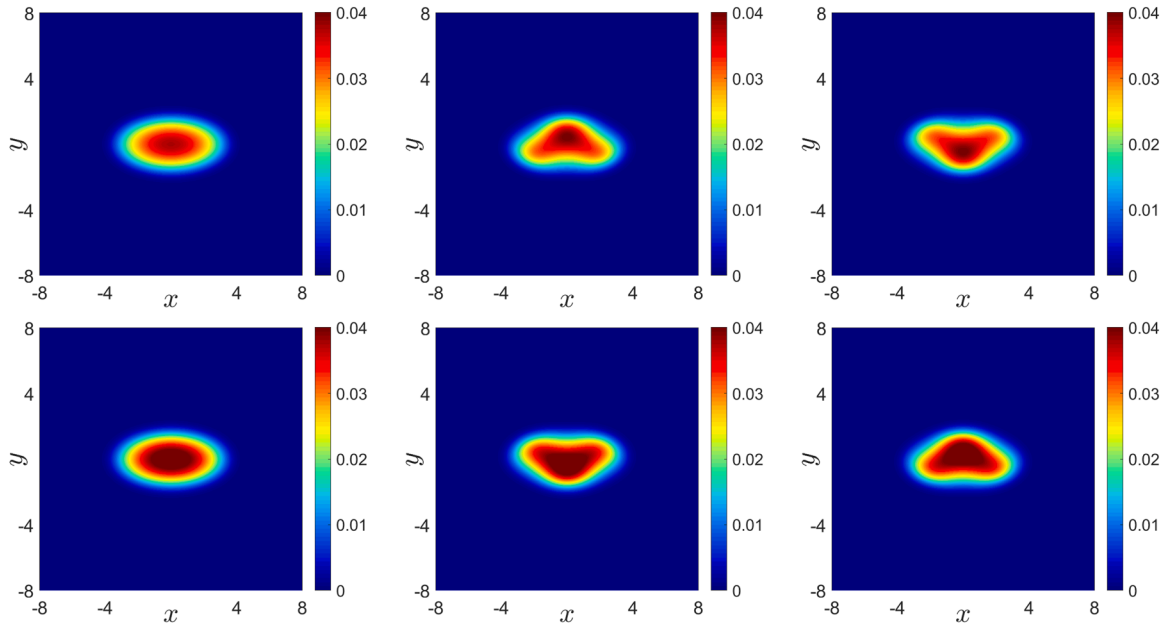

Fig. 3. Snapshots of the ground states $|\phi_j(\boldsymbol{x})|^2$ (left), perturbed densities $n_j^{\ell}(\boldsymbol{x}, t = 1.3)$ (middle) and $n_j^{\ell}(\boldsymbol{x}, t = 2.5)$ (right) by excitation mode indexed $\ell = 12$ for **Case II** in Example 3 ($j = 1$ (top), 2 (bottom)).

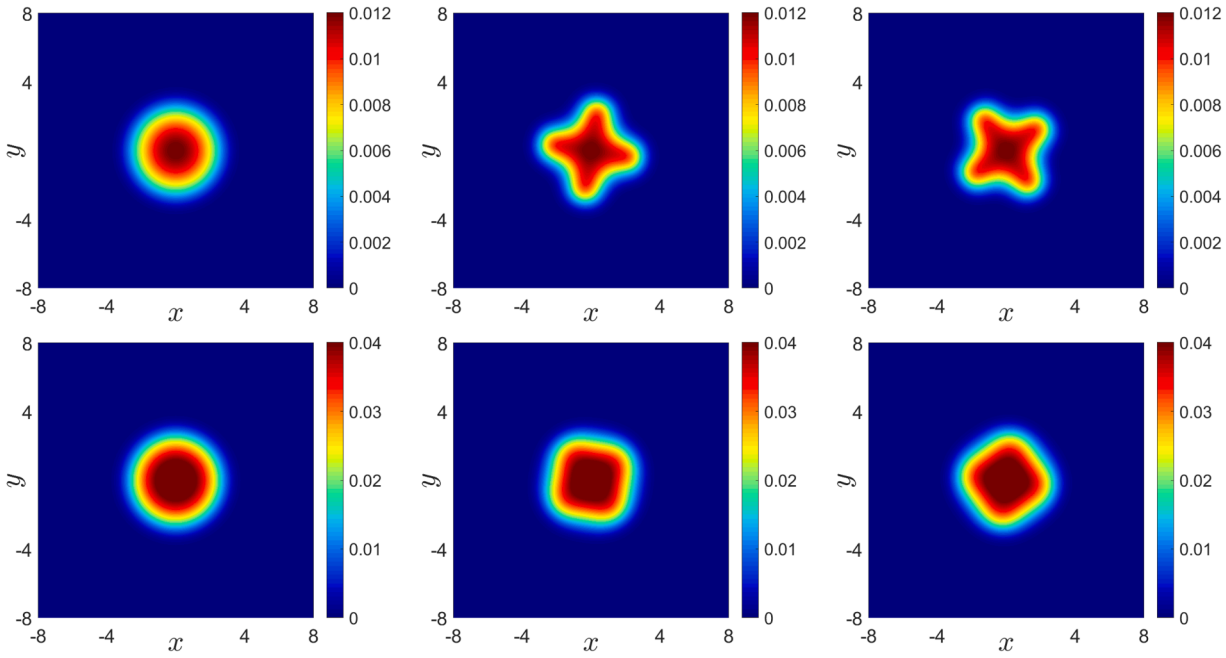

Fig. 4. Snapshots of the ground states $|\phi_j(\boldsymbol{x})|^2$ (left), perturbed densities $n_j^{\ell}(\boldsymbol{x}, t = 2)$ (middle) and $n_j^{\ell}(\boldsymbol{x}, t = 4)$ (right) by excitation mode indexed $\ell = 14$ for **Case III** in Example 3 ($j = 1$ (top), 2 (bottom)).

4.3. Applications of 3D cases

In this subsection, we investigate the excitation spectrum and Bogoliubov amplitudes of the BdG equations of two-component condensates. To visualize a normal mode, we show the isosurface plots of the Bogoliubov amplitudes. The numerical computation is carried out with a very fine mesh $h = 1/8$.

Example 4. We study the Bogoliubov amplitudes of the BdG equations of two-component condensates with/without a Josephson junction in 3D. In this example, we study the following four cases:

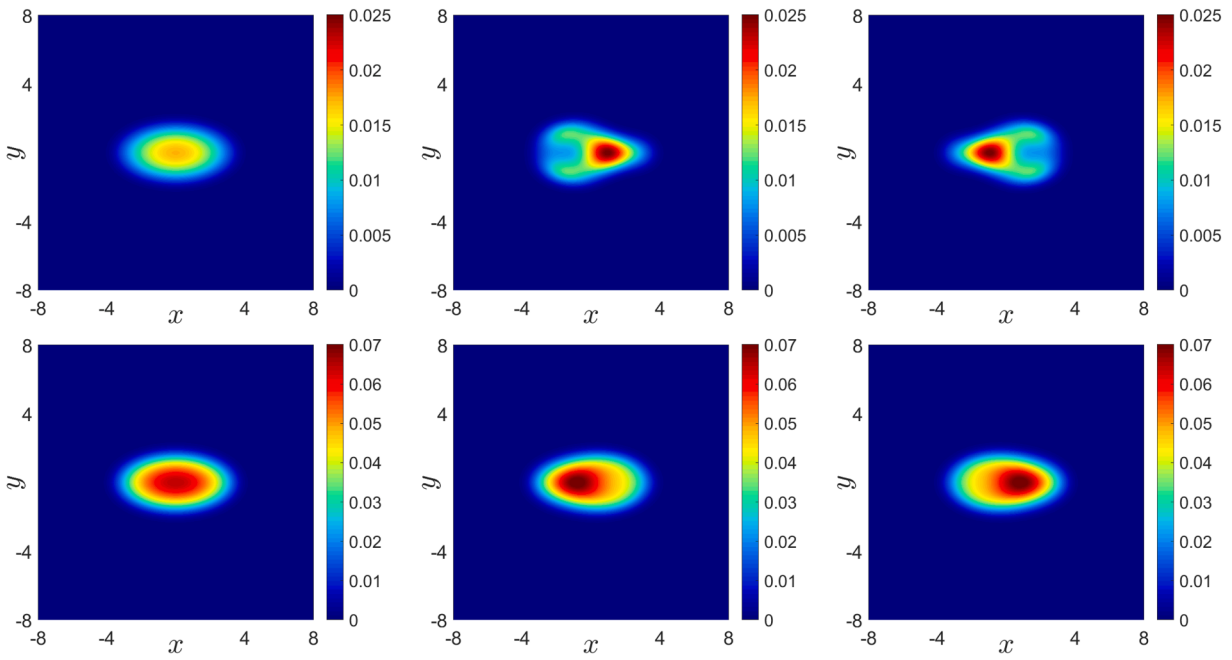

Fig. 5. Snapshots of the ground states $|\phi_j(\boldsymbol{x})|^2$ (left), perturbed densities $n_j^{\ell}(\boldsymbol{x}, t = 5.4)$ (middle) and $n_j^{\ell}(\boldsymbol{x}, t = 6.8)$ (right) by excitation mode indexed $\ell = 16$ for **Case IV** in Example 3 ($j = 1$ (top), 2 (bottom)).

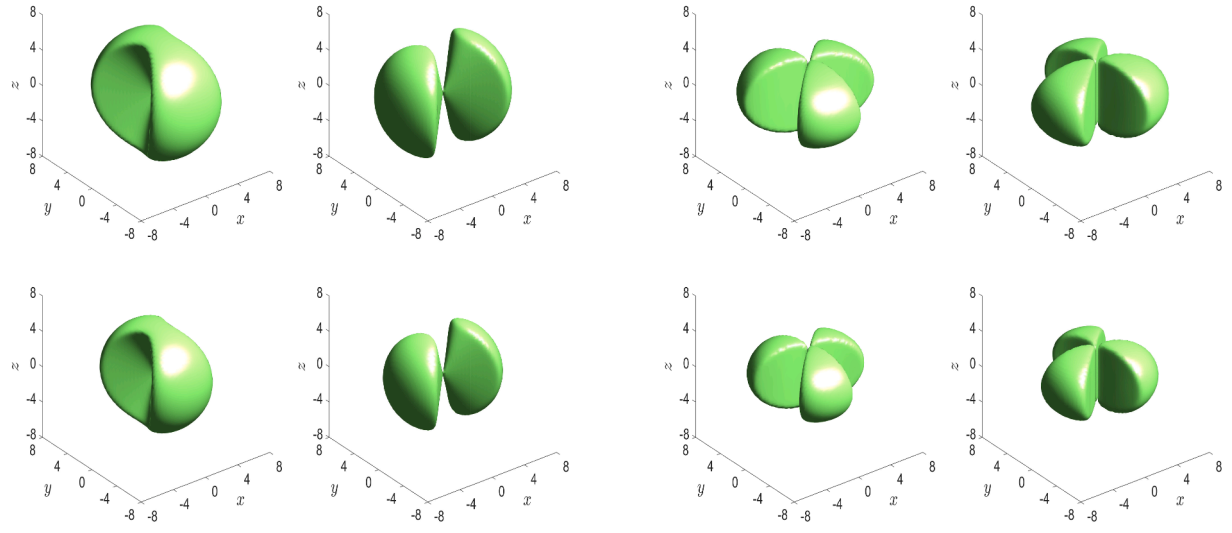

(a) **Case I**: u_1^{12}, u_2^{12} (top) and v_1^{12}, v_2^{12} (bottom). (b) **Case II**: u_1^{12}, u_2^{12} (top) and v_1^{12}, v_2^{12} (bottom).

Fig. 6. Isosurface plots of the Bogoliubov amplitudes ($u_j^{\ell} = 10^{-8}, v_j^{\ell} = 10^{-8}$) for **Case I & II**.

Case I. $\Omega = 1$, $\gamma_x = \gamma_y = \gamma_z = 1$, $\ell = 12$;
Case II. $\Omega = 1$, $\gamma_x = \gamma_y = \gamma_z/2 = 1$, $\ell = 12$;
Case III. $\Omega = 0$, $\gamma_x = \gamma_y = \gamma_z = 1$, $\ell = 7$;
Case IV. $\Omega = 0$, $\gamma_x = \gamma_y = \gamma_z/2 = 1$, $\ell = 7$.

Figs. 6 and 7 display isosurface plots of the eigenmodes $\boldsymbol{u}^{\ell} = (u_1^{\ell}, u_2^{\ell})^{\top}$ and $\boldsymbol{v}^{\ell} = (v_1^{\ell}, v_2^{\ell})^{\top}$ associated with the different ℓ for **Case I–II** and **Case III–IV** in Example 4, respectively. From these figures, we can see that the external potential affects the shape of the eigenmodes $\boldsymbol{u}^{\ell}$ and $\boldsymbol{v}^{\ell}$ obviously. It seems that the isosurface plots of the 1 and 2 components are complementary to each other. Meanwhile, all eigenmodes will be compressed along the direction with a larger trapping frequency. The presence of Josephson

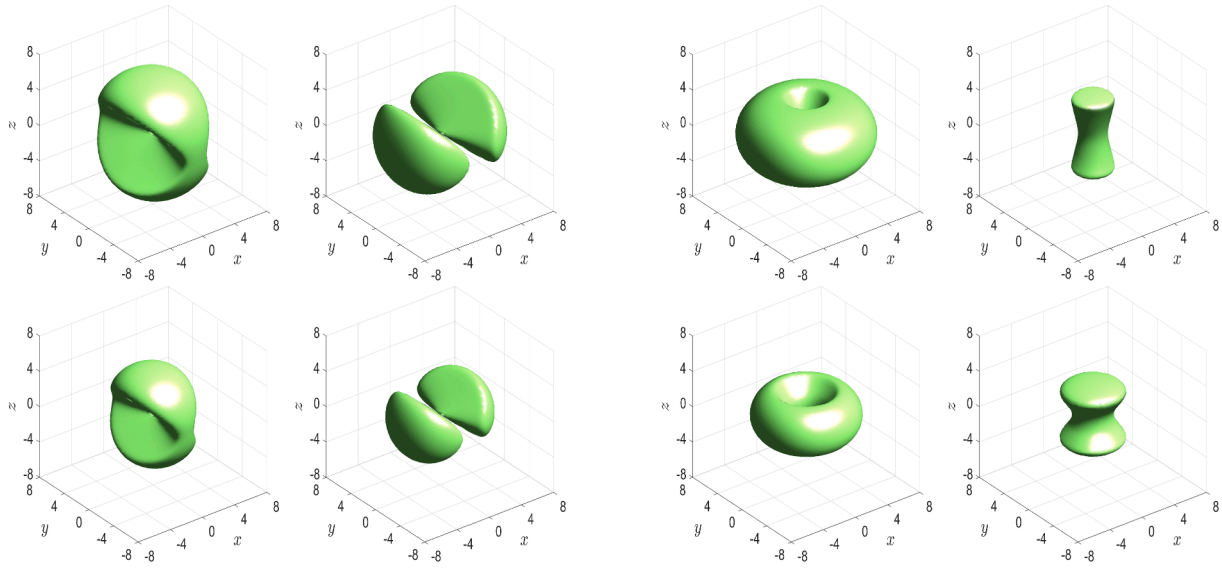

(a) **Case III**: u_1^7, u_2^7 (top) and v_1^7, v_2^7 (bottom). (b) **Case IV**: u_1^7, u_2^7 (top) and v_1^7, v_2^7 (bottom).

Fig. 7. Isosurface plots of the Bogoliubov amplitudes ($u_j^\epsilon = 10^{-8}, v_j^\epsilon = 10^{-8}$) for **Case III & IV**.

junction and isotropic/anisotropic external potential brings in many rich phase diagrams for eigenmodes, and we shall leave this topic as a future study.

5. Conclusion

In this work, we introduce a novel and highly efficient numerical method for solving the Bogoliubov-de Gennes (BdG) equations governing two-component BEC. We first explore its analytical properties, including the exact eigenpairs, structure of generalized nullspace, and bi-orthogonality of eigenspaces at a continuous level. Then, by combining the Fourier spectral method and the modified Gram-Schmidt bi-orthogonal algorithm, we propose a structure-preserving eigenvalue method for the resulting large-scale dense non-Hermitian discrete eigenvalue problem. Particularly, we incorporate the generalized nullspace to deal with the notorious slow-convergence or even divergence phenomena caused by eigenvalue zero, and achieved better numerical stability, convergence and efficiency. We design an interactive interface for users to provide matrix-vector multiplication (or the operator-function evaluation), therefore, no explicit matrix storage is required anymore, and it allows for efficient computations of large-scale and dense problems. Specifically, the operator-function evaluation is implemented with a near-optimal complexity $\mathcal{O}(N_t \log(N_t))$ thanks to FFT. Extensive numerical results are presented to showcase its superiority in terms of accuracy and efficiency. We then investigate the excitation spectrum (eigenvalues) and Bogoliubov amplitudes (eigenfunctions) around the ground state under different setups. It is worth pointing out that we can easily extend our solver to BdG excitations associated with different BEC, for example, the multi-component and spinor-dipolar BEC, with merely minor adjustments to the specific matrix-vector multiplication.

CRediT authorship contribution statement

Manting Xie: Writing – review & editing, Writing – original draft, Software, Investigation, Data curation; **Yong Zhang:** Writing – review & editing, Writing – original draft, Supervision, Methodology.

Data availability

Data will be made available on request.

Declaration of competing interest

The authors declare that they have no known competing financial interests or personal relationships that could have appeared to influence the work reported in this paper.

Acknowledgement

We want to thank Dr. Yu Li for his help with BOSP implementation. This work was partially supported by the National Natural Science Foundation of China (Nos. 12571437, 12271400), the National Key R&D Program of China (No. 2024YFA1012803), and the Basic Research Fund of Tianjin University (No. 2025XJ21-0010).

References

[1] C.J. Myatt, E.A. Burt, R.W. Ghrist, E.A. Cornell, C.E. Wieman, Production of two overlapping Bose-Einstein condensates by sympathetic cooling, Phys. Rev. Lett. 78 (4) (1997) 586–589.
[2] S. Ashhab, C. Lobo, External Josephson effect in Bose-Einstein condensates with a spin degree of freedom, Phys. Rev. A 66 (1) (2002) 013609.
[3] M.R. Matthews, D.S. Hall, D.S. Jin, J.R. Ensher, C.E. Wieman, E.A. Cornell, F. Dalfovo, C. Minniti, S. Stringari, Dynamical response of a Bose-Einstein condensate to a discontinuous change in internal state, Phys. Rev. Lett. 81 (2) (1998) 243–247.
[4] T. Ohmi, K. Machida, Bose-Einstein condensation with internal degrees of freedom in alkali atom gases, J. Phys. Soc. Jpn. 67 (1998) 1822–1825.
[5] J. Stenger, S. Inouye, D.M. Stamper-Kurn, H.-J. Miesner, A.P. Chikkatur, W. Ketterle, Spin domains in ground-state Bose-Einstein condensates, Nature 396 (6709) (1998) 345–348.
[6] J. Williams, R. Walser, J. Cooper, E. Cornell, M. Holland, Nonlinear Josephson-type oscillations of a driven two-component Bose-Einstein condensate, Phys. Rev. A 59 (1) (1999) R31–R34.
[7] W. Bao, Y. Cai, Ground states of two-component Bose-Einstein condensates with an internal atomic Josephson junction, East Asian J. Appl. Math. 1 (1) (2011) 49–81.
[8] W. Bao, Y. Cai, Mathematical models and numerical methods for spinor Bose-Einstein condensates, Commun. Comput. Phys. 24 (4) (2018) 899–965.
[9] H. Wang, Numerical simulations on stationary states for rotating two-component Bose-Einstein condensates, J. Sci. Comput. 38 (2009) 149–163.
[10] I. Bloch, J. Dalibard, W. Zwerger, Many-body physics with ultracold gases, Rev. Mod. Phys. 80 (3) (2008) 885–964.
[11] D. Baillie, R.M. Wilson, P.B. Blakie, Collective excitations of self-bound droplets of a dipolar quantum fluid, Phys. Rev. Lett. 119 (25) (2017) 255302.
[12] S.-X. Deng, T. Shi, S. Yi, Spin excitations in dipolar spin-1 condensates, Phys. Rev. A 102 (1) (2020) 013305.
[13] Y. Gao, Y. Cai, Numerical methods for Bogoliubov-de Gennes excitations of Bose-Einstein condensates, J. Comput. Phys. 403 (2020) 109058.
[14] J.A.M. Huhtamäki, P. Kuopanportti, Elementary excitations in dipolar spin-1 Bose-Einstein condensates, Phys. Rev. A 84 (4) (2011) 043638.
[15] D.S. Jin, J.R. Ensher, M.R. Matthews, C.E. Wieman, E.A. Cornell, Collective excitations of a Bose-Einstein condensate in a dilute gas, Phys. Rev. Lett. 77 (3) (1996) 420–423.
[16] C. Boccato, C. Brennecke, S. Cenatiempo, B. Schlein, Bogoliubov theory in the Gross-Pitaevskii limit, Acta. Math. 222 (2019) 219–335.
[17] B. Hu, G. Huang, Y. Ma, Analytical solutions of the Bogoliubov-de Gennes equations for excitations of a trapped Bose-Einstein-condensed gas, Phys. Rev. A 69 (6) (2004) 063608.
[18] S. Stringari, Collective excitations of a trapped Bose-condensed gas, Phys. Rev. Lett. 77 (12) (1996) 2360–2363.
[19] R.B. Lehoucq, D.C. Sorensen, C. Yang, ARPACK Users'Guide: Solution of Large Scale Eigenvalue Problems with Implicitly Restarted Arnoldi Methods, SIAM, Philadelphia, 1998.
[20] I. Danaila, M.A. Khamehchi, V. Gokhroo, P. Engels, P.G. Kevrekidis, Vector dark-antidark solitary waves in multicomponent Bose-Einstein condensates, Phys. Rev. A 94 (5) (2016) 053617.
[21] M. Edwards, P.A. Ruprecht, K. Burnett, R.J. Dodd, C.W. Clark, Collective excitations of atomic Bose-Einstein condensates, Phys. Rev. Lett. 77 (9) (1996) 1671–1674.
[22] Q. Tang, M. Xie, Y. Zhang, Y. Zhang, A spectrally accurate numerical method for computing the Bogoliubov-de Gennes excitations of dipolar Bose-Einstein condensates, SIAM J. Sci. Comput. 44 (1) (2022) B100–B121.
[23] Z. Bai, R.C. Li, Minimization principles for the linear response eigenvalue problem I: theory, SIAM J. Matrix Anal. Appl. 33 (4) (2012) 1075–1100.
[24] Z. Bai, R.C. Li, Minimization principles for the linear response eigenvalue problem II: computation, SIAM J. Matrix Anal. Appl. 34 (2) (2013) 392–416.
[25] Y. Zhang, X. Liu, M. Xie, Efficient and accurate computation of the Bogoliubov-de Gennes excitations for the quasi-2D dipolar Bose-Einstein condensates, East Asian J. Appl. Math. 11 (4) (2021) 686–707.
[26] L. Chen, H. Pu, Z.-Q. Yu, Y. Zhang, Collective excitation of a trapped Bose-Einstein condensate with spin-orbit coupling, Phys. Rev. A 95 (3) (2017) 033616.
[27] G. Sadaka, V. Kalt, I. Danaila, F. Hecht, A finite element toolbox for the Bogoliubov-de Gennes stability analysis of Bose-Einstein condensates, Comput. Phys. Commun. 294 (2024) 108948.
[28] Y. Li, Z. Wang, Y. Zhang, Bi-Orthogonal Structure-Preserving eigensolver for large-scale linear response problem, Technical Report, arXiv preprint arXiv:2506.08355, 2025.
[29] Y. Li, Z. Li, M. Xie, Y. Zhang, An efficient Fourier spectral algorithm for the Bogoliubov-de Gennes excitation eigenvalue problem, Technical Report, arXiv preprint arXiv:2506.08308, 2025.
[30] W. Bao, H. Wang, A mass and magnetization conservative and energy-diminishing numerical method for computing ground state of spin-1 Bose-Einstein condensates, SIAM J. Numer. Anal. 45 (5) (2007) 2177–2200.
[31] W. Liu, Y. Cai, Normalized gradient flow with Lagrange multiplier for computing ground states of Bose-Einstein condensates, SIAM J. Sci. Comput. 43 (1) (2021) B219–B242.
[32] T. Tian, Y. Cai, X. Wu, Z. Wen, Ground states of spin-F Bose-Einstein condensates, SIAM J. Sci. Comput. 42 (4) (2020) B983-B1013.
[33] X. Antoine, Q. Tang, Y. Zhang, A preconditioned conjugated gradient method for computing ground states of rotating dipolar Bose-Einstein condensates via kernel truncation method for dipole-dipole interaction evaluation, Commun. Comput. Phys. 24 (4) (2018) 966–988.
[34] L. Jia, A.-B. Wang, S. Yi, Low-lying excitations of vortex lattices in condensates with anisotropic dipole-dipole interaction, Phys. Rev. A 97 (4) (2018) 043614.
[35] M. Shao, F.H.D. Jornada, L. Lin, C. Yang, J. Deslippe, S.G. Louie, A structure preserving Lanczos algorithm for computing the optical absorption spectrum, SIAM J. Matrix Anal. Appl. 39 (2) (2018) 683–711.
[36] J. Shen, T. Tang, L.-L. Wang, Spectral Methods: Algorithms, Analysis and Applications, Springer, Berlin, 2011.
[37] Y. Li, M. Xie, S. Zhang, Y. Zhang, An efficient and spectrally-accurate solver for computing the Bogoliubov-de Gennes excitations of rotating Bose-Einstein condensates, 2026, Preprint.
[38] X. Liu, Q. Tang, S. Zhang, Y. Zhang, On optimal zero padding of kernel truncation method, SIAM J. Sci. Comput. 46 (1) (2024) A23–A49.